3. RESULTS

One of the main goals of this thesis was to receive further information about the molecular events that underlay scrapie, the oldest known prion disease. Two different methods were used (FTIRM and XRF Microprobe) as well as different organs of the scrapie infected animals (brain and dorsal root ganglia), and different time points during the disease were examined (pre-clinical, first clinical signs, terminal). Last but not least another disease causing a lethal encephalitis (Reovirus infected hamsters) was studied. The following aspects have been considered: First it was important to examine changes in protein composition throughout scrapie pathogenesis, and to correlate these findings with the structural changes associated with the PrP^{C} to PrP^{Sc} conversion. The identification of protein changes involved in the early pathogenesis of scrapie are important for understanding the disease process and for developing assays for early disease detection and treatment. Hence, orally 263K scrapie infected hamsters were studied at 4 different time points: 100 days post infection (dpi), 130 dpi, at first clinical signs (fcs, ~145 dpi) and at the terminal stage (~180 dpi) of the disease. The total protein, α-helical protein, and β-sheet protein contents and distributions were determined as a function of disease severity and correlated with PrP^{Sc} immunostaining (see chapter 3.1). It was shown earlier (Kneipp *et al.*, 2003) that neurons of terminally 263K infected hamster dorsal root ganglia had elevated β-sheet. These alterations were mainly detected at the cell membrane. In a FTIRM pathogenesis study performed on brain sections of scrapie infected hamsters, it was demonstrated that already at the earliest investigated time point, 90 dpi, reproducible differences in first derivative spectra of the DMNV could be detected (Kneipp *et al.*, 2002). To determine whether it is possible to detect changes at even earlier stages in the disease, the DMNV of 16 infected and 8 control animals at 70 days post infection was studied accordingly (see chapter 3.2) and with a synchrotron based spectrometer, providing higher signal-to-noise ratios. Furthermore, the discovery of spectral changes inevitably leads to the question of their specificity. Addressing this, two different experiments were performed. First, dorsal root ganglia of different scrapie strains, 263K and ME7, were examined using a focal plane array (see chapter 3.3). Second, the DMNV of seven reovirus T3C9 infected and six age matched control hamsters was investigated (see chapter 3.4) and spectral changes were compared to those of terminally infected 263K scrapie animals (see chapter 3.5). Finally, the role of metals

in scrapie pathogenesis was studied by XRF microprobe. The same samples that were investigated in the pathogenesis study were used to shed light onto the relation between metal ions such as copper, iron and zinc to the misfolded prion protein (see chapter 3.6).

3.1 Spectral changes in DRG of 263K scrapie-infected hamsters

The Amide I protein band can be deconvolved into six to nine components representative of the different secondary structure motifs in a protein (Byler & Susi, 1986). The analysis of β-sheet and α-helical protein content, respectively, was performed based on curve-fitting of the Amide I band, which is shown in **Figure 2.5** (see page 59). The integrated area between 1624 and 1628 cm^{-1} is proportional to the amount of β-sheet content while the integrated area between 1654 and 1658 cm^{-1} is proportional to the α-helical protein content. These regions were chosen because the respective part of the spectrum has the least overlap from other protein secondary structural components.

To examine changes in the secondary structure of proteins during scrapie pathogenesis, the mean values ± standard deviation for the β-sheet and α-helical content were calculated and plotted in **Figure 3.1.1**. **Figure 3.1.1A** shows the β-sheet content for infected (black bars) and control (white bars) hamster dorsal root ganglia at the four investigated time points. As a function of age, results showed that the β-sheet content remained constant in control hamsters, but increased in the scrapie-infected animals. The most dramatic difference between the control and infected animals was observed at 100 dpi, where the β-sheet content in scrapie-infected ganglia was significantly lower than in the control ganglia ($p=0.013$). Over the course of the disease, we found an increase in β-sheet protein content of about 8% from 100 dpi to the terminally-diseased state ($p=0.003$).

In contrast, the α-helical protein content was quite variable with age (**Figure 3.1.1B**). No significant differences were observed between the control and infected ganglia at each time point. At all stages except 100 dpi, the amount of α-helical protein was higher in the control animals. However, at 100 dpi, infected animals exhibited more α-helical protein than the control hamsters.

To determine whether the observed decrease in β-sheet was due to an increased expression of proteins low in β-sheet or the opposite, i.e. a decreased expression of proteins high in β-sheet, the relative protein content was determined by calculating the ratio of the protein content (integrated area of the amide I band) by the integrated region 2700 – 3700 cm^{-1}. This region contains NH, OH and CH bonds of all major biomolecules was therefore termed as 'total biomass', nevertheless providing only an estimation about the total protein content in the tissue. While the controls (**Figure 3.1.1C**, white bars) remained constant in relative protein content (with the exception of 130 dpi animals), the scrapie-infected animals (black bars) showed a significant increase in protein expression (p=0.020) at 100 dpi compared to control. Protein content then declined gradually during pathogenesis by ~16% and ends with significantly less total protein content at the terminal stage of the disease (p=0.013).

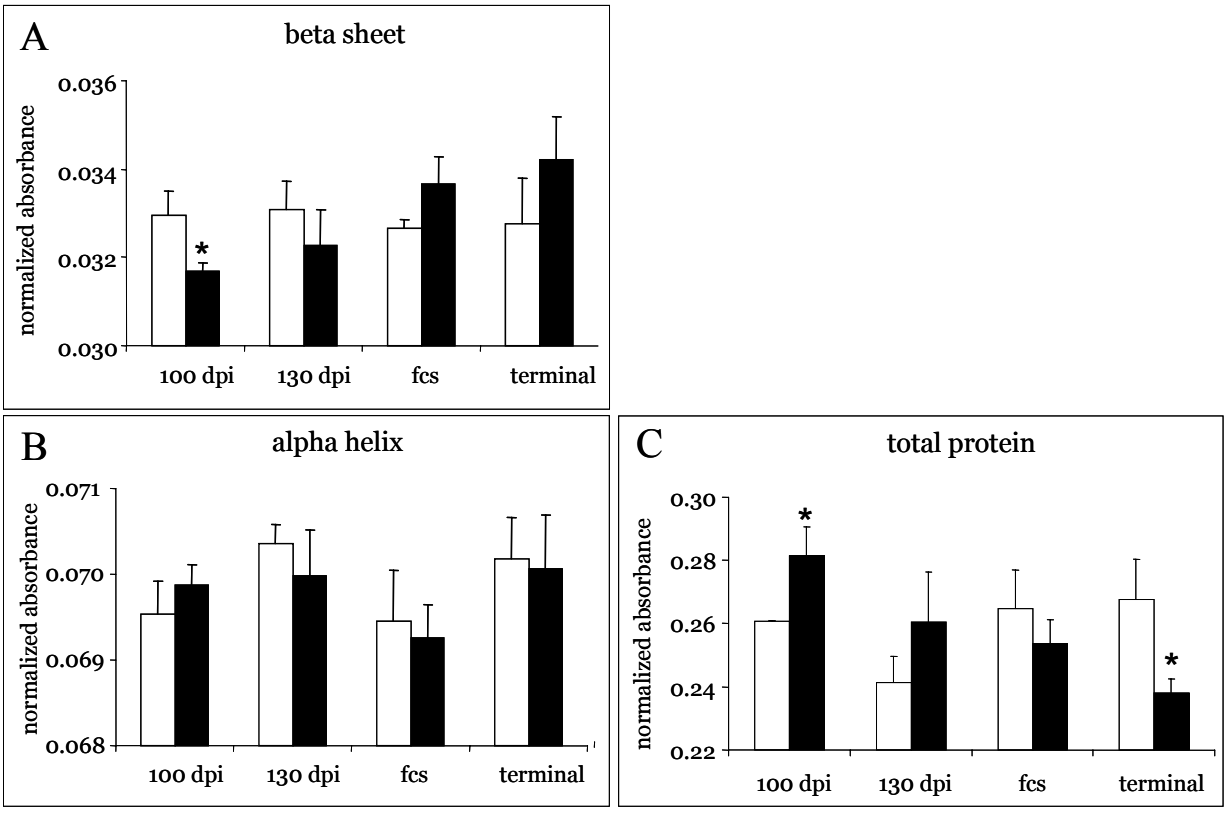

Figure 3.1.1: Mean values + average deviation for the (A) β-sheet, (B) α-helical and (C) total relative protein content for (black bars) infected and (white bars) control hamster dorsal root ganglia at the four investigated time points. Asterisks mark significant differences ($p<0.05$) between scrapie and control. Note the scale of the y-axis.

In additional to measuring β-sheet content, the distribution of β-sheet proteins within the tissue was examined. Photomicrographs and corresponding FTIRM images of the β-sheet distribution for representative control (left) and infected (right) ganglia at different time points are shown in **Figure 3.1.2A**. The color scale in the FTIRM images represents the relative β-sheet content, i.e. a value calculated by the ratio of the absorbance area between 1624 cm^{-1} and 1628 cm^{-1} divided by the total area of the amide I band, ranging from purple (≤0.03; very little β-sheet) to red (≥0.04; elevated β-sheet).

In all images, the β-sheet content was slightly higher near the cell membranes and extracellular matrix. For the control animals (**Figure 3.1.2A**, left columns), the FTIRM images appeared similar at each time point, indicating no significant change in β-sheet distribution or content over time. For the scrapie-infected animals, it can be seen that, with the progression of the disease, the images shift to higher values for β-sheet content, indicated by more green and red pixels. At pre-clinical time points, elevated β-sheet was detected exclusively near the cell membranes of only a few cells. Otherwise, these cells generally exhibited proteins lower in β-sheet content than the controls, as can be seen by the overall dark blue colored pixels. In addition, the cytoplasm of some neurons contained proteins extremely low in β-sheet which seemed to be accumulated in vesicle like circular structures (arrowheads). During disease progression, the number of affected cells increased such that, by the terminal stage, overall β-sheet content increased and was observed throughout a large number of cells, including but not limited to the cell membrane.

Spectra taken from areas representing low ($I_{\beta\text{-sheet}}$ = 0.033), medium ($I_{\beta\text{-sheet}}$ = 0.038) and high β-sheet content ($I_{\beta\text{-sheet}}$ = 0.045) are indicated by the numbers 1-3 in the chemical images (**Figure 3.1.2A**) and are shown in **Figure 3.1.2B**. The original spectra and 2nd derivatives are shown. The peak associated to α-helical structures gradually shifted and decreased from 1655 to 1652 cm^{-1}, while the peaks at 1683 and 1637 cm^{-1} (both attributed to β-sheet) increased. An additional peak appeared around 1624 cm^{-1}, indicating the presence of aggregated protein strands (Casal *et al.*, 1988; Dong *et al.*, 1995; Ismail *et al.*, 1992; Martinez *et al.*, 1996; Clark *et al.*, 1981; Damaschun *et al.*, 2000; Dornberger *et al.*, 1996).

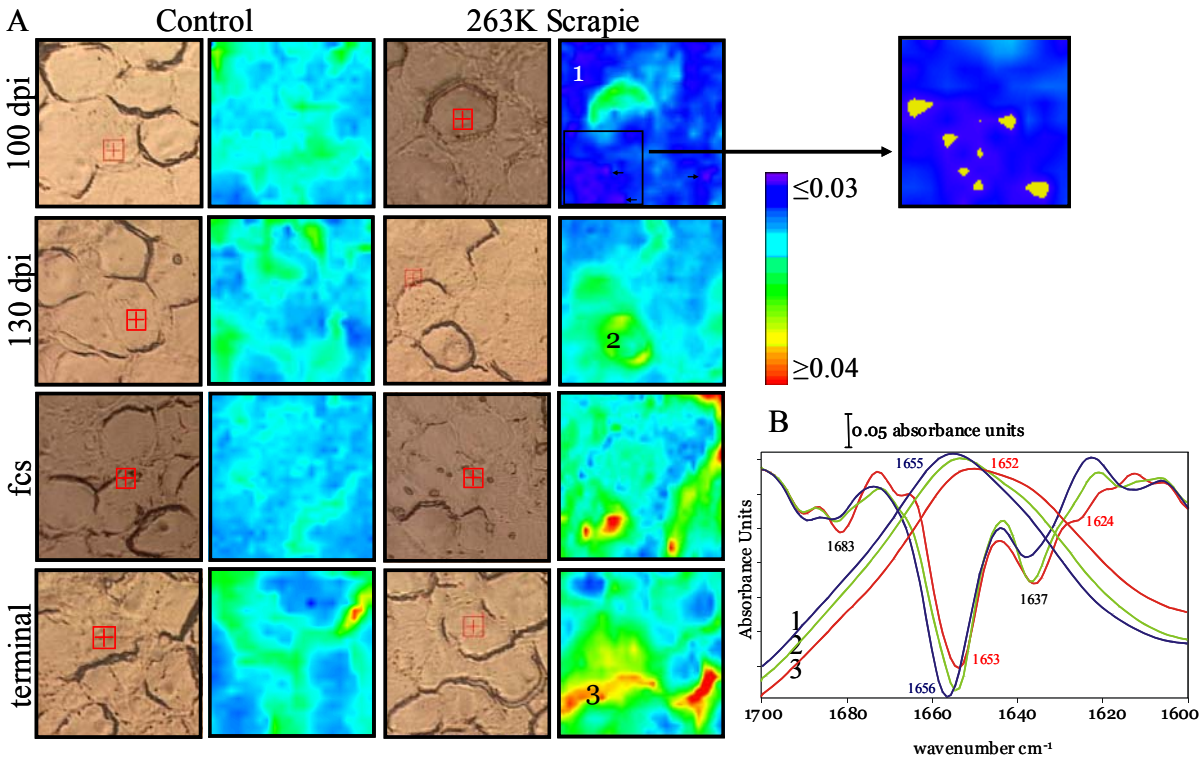

Figure 3.1.2: (A) Photomicrographs (1st and 3rd column) and corresponding FTIRM images (2nd and 4th column) of the β-sheet distribution for (left) control and (right) infected ganglia at different time points. Areas exhibiting extremely low β-sheet at 100 dpi are indicated by arrowheads. The area shown in the inset is shown in higher magnification to the right, for better contrast and visibility, purple pixel have been replaced by yellow. (B) Original and 2nd derivative spectra of areas indicated by numbers in the chemical maps. Red square in photomicrographs: 10x10 µm.

Since the FTIRM results showed an increase in β-sheet content as the disease progressed, which could be due to the misfolded prion protein, immunostaining with the 3F4 antibody for the prion protein was performed on adjacent tissue sections (**Figure 3.1.3**). A clear progression of PrP^{Sc} deposition during the pathogenesis was confirmed by the increased appearance of dark brown dots in neurons of the infected tissue. Since the antibody 3F4 stains both the cellular and the misfolded form of the prion protein (Kascsak *et al.*, 1987), an overall brown color can be seen in all animals, where the intensity does not change between time points or infection state. In 263K infected hamsters, it is known that PrP^{Sc} accumulates as micro disperse aggregates, so the dark brown dots, which only appear in infected tissue, are generally interpreted as the misfolded protein. At 100 dpi, very few neurons and satellite cells stained positive for PrP^{Sc}, whereas prion protein accumulation was gradually more evident during pathogenesis, as indicated by the increasing number of small brown dots.

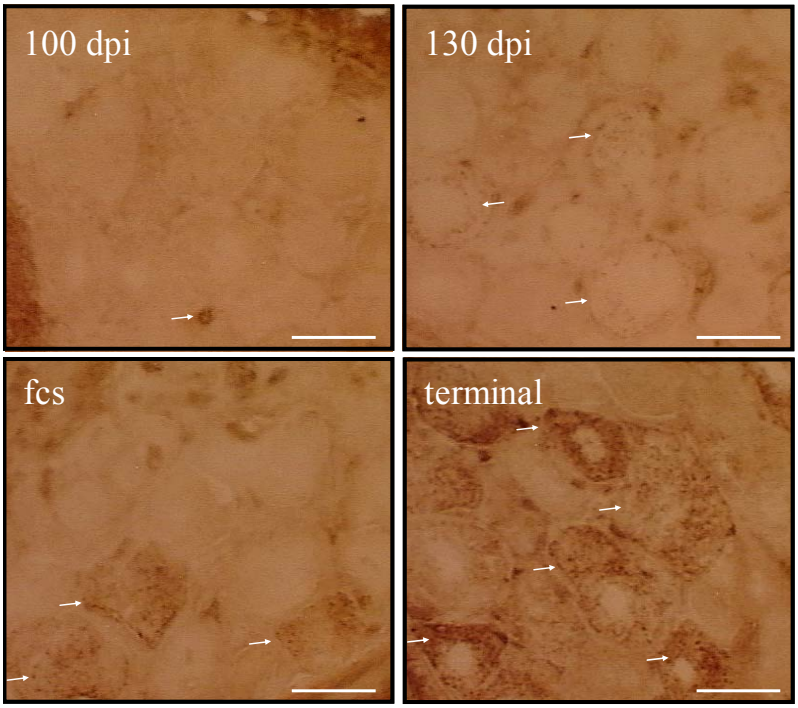

Figure 3.1.3: Photomicrographs of the antibody 3F4 stained adjacent sections. PrP^{Sc} can be detected as dark brown dots in a number (arrows) but not all of the cells at later time points. Scale bar: 30 µm

To directly correlate elevated β-sheet content with aggregated PrP^{Sc} distribution, the FTIRM samples were subsequently stained with the monoclonal antibody, 3F4. **Figure 3.1.4** shows the results of an infected animal at 100 dpi (left column) and at first clinical signs (right column). The first row displays the unstained photomicrographs. The photomicrographs in the second row show the same tissue stained with the prion-specific antibody, 3F4. The third and fourth row represents the β-sheet and α-helix distributions, respectively, as measured with FTIRM. At 100 dpi, the immunostained section showed no evidence of PrP^{Sc} inside the cells, but in some of the surrounding satellite cells (arrows). The FTIRM image of the same area also showed a higher amount of β-sheet. At fcs, some cells stained positive for PrP^{Sc} (as can be seen by dark brown dots) and showed a high content of β-sheet in the corresponding spectra. In contrast, the cell shown in the upper left of the fcs photomicrograph showed elevated β-sheet but no PrP^{Sc} staining, indicating that β-sheet rich proteins other than PrP^{Sc} also increase during pathogenesis.

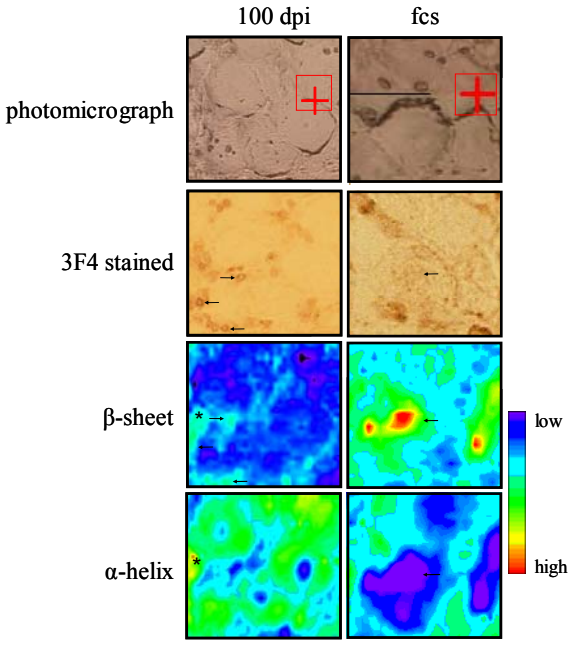

Figure 3.1.4: Comparison of the results from the FTIRM of an infected animal at (left) 100 dpi and (right) first clinical signs with 3F4 stained section of the same tissue. Photomicrographs of the areas investigated with FTIRM are shown in the 1st row (unstained) and 2nd row (3F4-antibody stained). The β-sheet and α-helix distributions are represented in the 3rd and 4th rows, respectively. At 100 dpi, some areas show high β-sheet as well as high α-helix (*), which was not observed at the terminal stage. Areas with PrP^{Sc} deposition as seen in the 3F4 stained sections showed elevated β-sheet (arrows). Red square in photomicrographs: 10x10 µm.

A statistical analysis of the FTIRM images showed that the pixel correlation between α-helix and β-sheet content was low at early time points (100 dpi, R^2 = 0.267) but increased during pathogenesis (130 dpi, R^2 = 0.338; fcs, R^2 = 0.345; terminal, R^2 = 0.636) (**Figure 3.1.5**), suggesting that, as the disease progressed, α-helical rich proteins were replaced by and/or converted to β-sheet rich proteins. The lower correlation can also be seen at 100 dpi in **Figure 3.1.4**, which shows relatively high β-sheet in the same area as high α-helix (indicated by an asterisk).

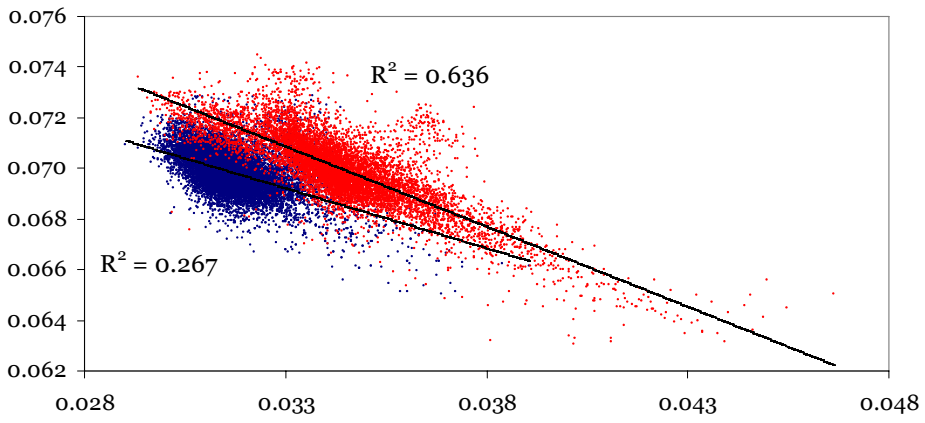

Figure 3.1.5: Correlation of β-sheet to α-helix content in scrapie-infected DRG at (blue) 100 dpi and (red) terminal stage.

Spectral indicators for changes in the lipid composition were analyzed by calculating the ratio of the peak intensities at 2957 cm^{-1} (asymmetric CH_3 stretching vibrations of lipids) and 2925 cm^{-1} (asymmetric CH_2 stretching vibrations of lipids), using a baseline in the range 2838 – 3000 cm^{-1}. The higher the ratio, the shorter is the lipid chain length (or the more branched chains). The ratio of the CH_3/CH_2 peak intensities was plotted for the different time points in **Figure 3.1.6A**. Control animals exhibited similar ratios at all time points, indicating that the lipid composition does not change over the investigated time. While no differences between scrapie and control were detected at 100 dpi, 130 dpi infected animals exhibited a slight decrease in the CH_3/CH_2 ratio (from 0.568 in control to 0.561 in infected animals). At fcs, the ratio dropped from 0.569 in controls to 0.543 in infected animals. The high standard deviations at 130 dpi and fcs are due to individual differences in the infected animals. At 130 dpi, for example, four of the five infected animals exhibited ratios similar or higher than those of the controls (0.595, 0.573, 0.560 and 0,586 compared to an average of 0.568 in controls), while one animal (H100.36) had a ratio of only 0.491. At fcs, two of the four animals exhibited similar values compared to control (0.575 and 0.559), while the other two animals showed decreased values (0.526 and 0.514 compared to a mean value of 0.569 in control). This indicates that lipid composition changes during the coarse of the disease, starting between 100 and 130 dpi with increased values, i.e. shorter fatty acid chains. Later, between 130 and 145 dpi, longer fatty acid chains predominate (therefore smaller ratios) and towards the end of the disease, control and infected animals level off again, exhibiting only slightly less ratios in infected animals. In summary, the examination of the lipid composition indicates that, besides the accumulation of misfolded prion protein and the up- and down-regulation of genes, the fatty acid metabolism in scrapie infected animals is altered, already at preclinical time points.

Finally, the fingerprint region was analyzed by calculating the ratio of the integrated peak absorbencies between 1149 – 980 cm^{-1} and 1350 – 1151 cm^{-1} (**Figure 3.1.6B**). These regions are dominated by carbohydrates, phospholipids and nucleic acids. It was shown that control animals did not change over time. Although no significant changes at any time point between scrapie and control could be detected, at 100 dpi, infected animals showed increased ratios, from 1.45 in control to 1.80 in infected animals, while at 130 dpi, a significant decrease ($p=0.0084$, compared to 100 dpi scrapie) occurred. Interestingly, H100.36, exhibiting the lowest ratio in lipid

composition, showed the highest value in the calculation of the fingerprint region (1.593 compared to 0.851, 0.597, 1.228 and 0.979). At fcs, values increased again and did not change dramatically until the end of the disease anymore. In summary, starting at ~100 dpi, infected animals exhibited increased values, indicating changes in nucleic acids, phospholipids and carbohydrates, then dropped to lower values at around 130 dpi before they increased again. The animal H100.36 might have been in a more progressed stage of the disease compared to the other four 130 dpi infected animals, since the lipid composition and the fingerprint region exhibited values closer to those of animals at fcs. Since only 5 animals each group have been investigated, only a tentative interpretation can be made.

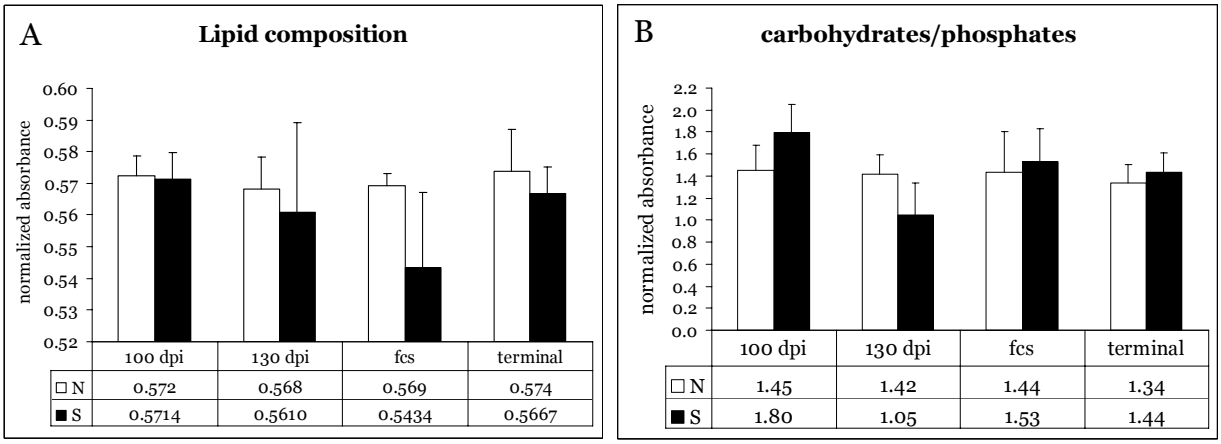

	100 dpi	130 dpi	fcs	terminal
□ N	0.572	0.568	0.569	0.574
■ S	0.5714	0.5610	0.5434	0.5667

	100 dpi	130 dpi	fcs	terminal
□ N	1.45	1.42	1.44	1.34
■ S	1.80	1.05	1.53	1.44

Figure 3.1.6: Mean values + average deviation for the (A) CH_3/CH_2 ratio and (B) results of the carbohydrate/phosphate region for (black bars) infected and (white bars) control hamster dorsal root ganglia at the four investigated time points. Note the scale of the y-axis.

3.2 DMNV of 263K infected hamsters at 70 dpi

As had been demonstrated in an earlier study, first derivative spectra of the DMNV of terminally 263K infected hamster showed dramatic differences in the fingerprint region compared to control animals (Kneipp *et al.*, 2002). Although less and with smaller intensities, changes were already seen at 90 days post infection in the region 1100 – 1000 cm^{-1}, indicating changes in complex ring vibrations of carbohydrates. Since the accumulation of misfolded prion protein could be detected in all four examined hamsters at 69 days post infection (McBride *et al.*, 2001), it might be possible to find scrapie related spectral features at even earlier time points than 90 dpi. Therefore, sixteen 263K infected (S1 – S16) and eight control animals (N1 – N8) were sacrificed and examined 70 days after infection. **Figure 3.2.1** shows 3F4

immunostained adjacent sections of one infected (left) and one control animal (right) 70 days post infection. In the top row, areas of the DMNV are shown in the upper part of the picture compared to the HypN in the lower part. In scrapie infected animals, three of five infected animals showed slightly darker brown coloring in the DMNV. Moreover, four of five animals exhibited alterations in tissue structure of the DMNV, as can be seen in higher magnification in the bottom row.

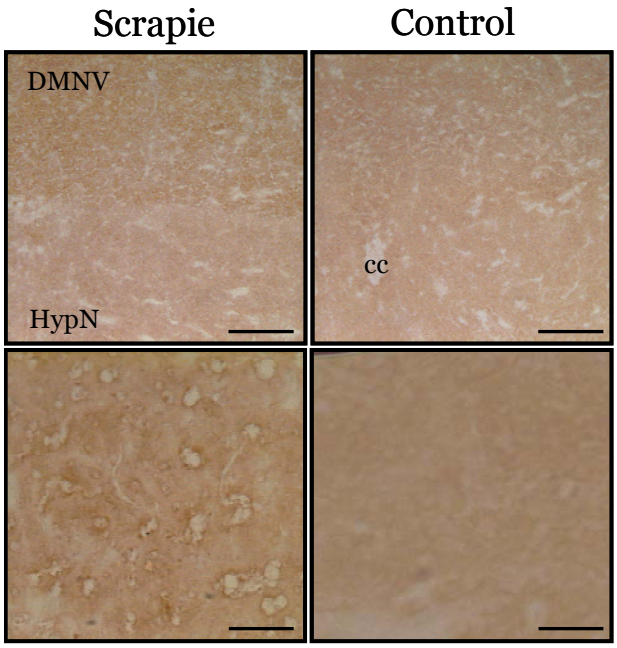

Figure 3.2.1: 3F4 immunostained adjacent sections of the DMNV of an infected (left) and a control animal (right) at 70 dpi. The bottom row shows parts of the DMNV from the upper pictures in higher magnification. Scale bars: 100 µm (top row), 20 µm (bottom row)

To analyze the molecular composition of the DMNV, overview measurements covering big areas of the Medulla oblongata (areas of the DMNV, the HypN, the area postrema, and parts of the white matter) were carried out to identify the different structures within the tissue based on the protein/lipid-ratio. The DMNV (together with the SolN) is high in protein and can be distinguished from the surrounding lipid rich white matter (see **Figure 3.4.1** in Reovirus infected brain tissue). Subsequent higher detailed maps were recorded on the identified areas of the DMNV in the overview images. Cluster analysis of first derivative spectra in the range 1300 – 1000 cm^{-1} separated the area of the DMNV from the attached HypN. A dendrogram of the result of a cluster analysis and the corresponding average spectra of the two structures from an infected animal is shown in **Figure 3.2.2**. Note the high heterogeneity between the two groups compared to the small heterogeneity within the groups.

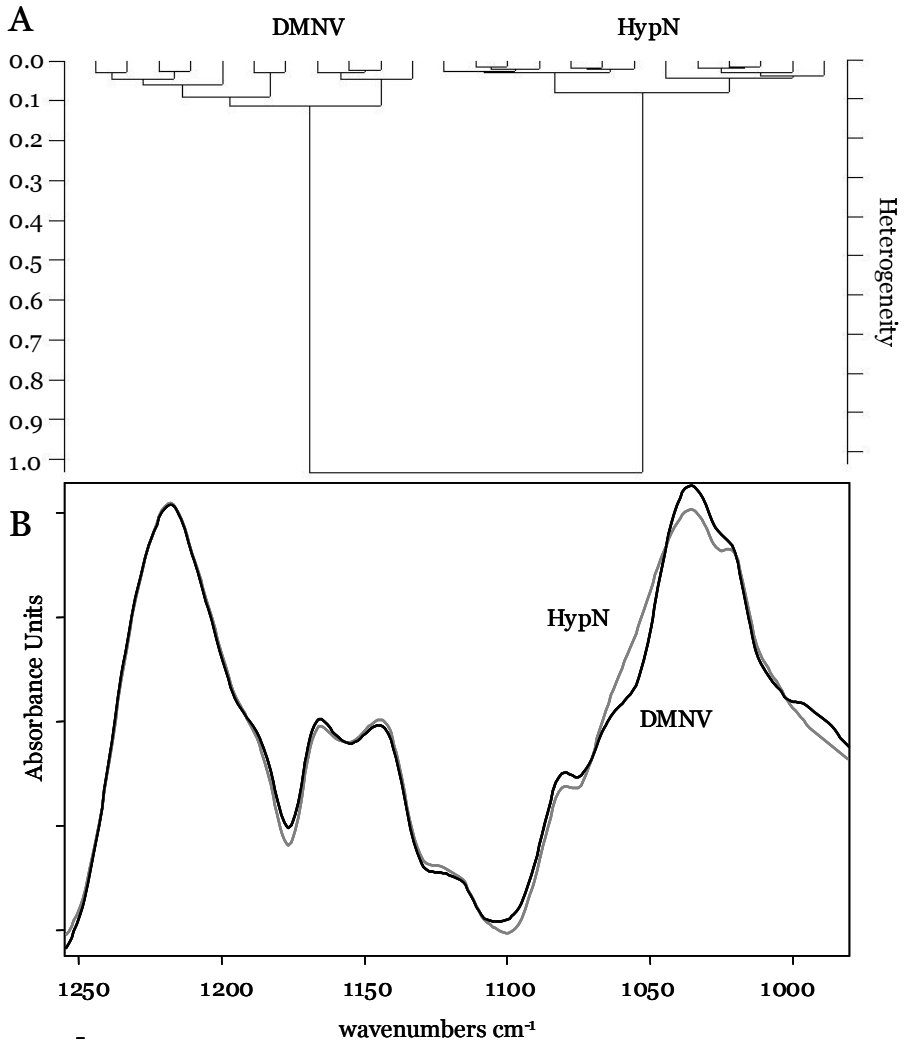

Figure 3.2.2: A. dendrogram shown as a result of the Cluster Analysis performed on the detailed measurement of an infected animal at 70 dpi in the range 1300 – 1000 cm^{-1}. B. First derivative average spectra of the DMNV (black) and HypN (grey) in the region 980 – 1250 cm^{-1} .

Cluster analyses were applied to the extracted spectra of all high detailed maps from the sixteen infected and eight control animals (**Figure 3.2.3A**). Note that the heterogeneity here is much smaller than in **Figure 3.2.2A**. Average spectra of the DMNV are shown in **Figure 3.2.3B**. Here, 1st derivative spectra of 263K infected (black) and control animals (gray) are plotted in the region 1250 – 980 cm^{-1}. It can be seen that differences in the average spectra are minimal which is also reflected in the low heterogeneity in the dendrogram and the fact that the animals do not cluster into distinct groups based on their infection status. However, minimal changes can be seen in the region between 1100 and 1000 cm^{-1}, which is due to alterations in complex sugar ring vibrations of carbohydrates.

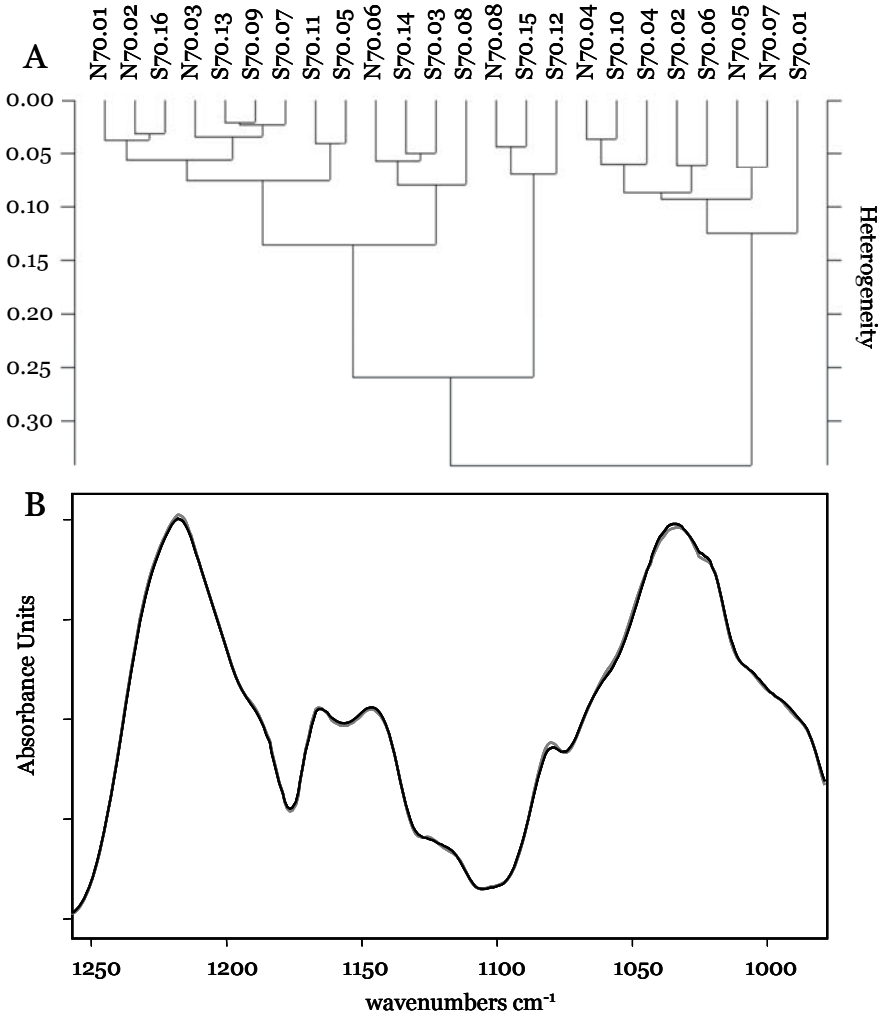

Figure 3.2.3: A. dendrogram shown as a result of the Cluster Analysis of normalized first derivative spectra of the DMNV of 16 infected (S01-S16) and 8 control animals (N01-N08) at 70 dpi in the range 1100 – 1000 cm^{-1}. B. Average of 16 263K infected (black) and 8 control animals (grey).

As was shown by Kneipp (Kneipp *et al.*, 2002), the molecular changes observed at 90 dpi, and here at 70 dpi, are becoming more obvious during the course of the disease, as can be seen in **Figure 3.2.4**. Here, average spectra of infected (red) and control (blue) animals are shown for the time points 70 dpi, 90 dpi, 120 dpi and at the terminal stage of the disease (from bottom to top). Although only one animal is displayed for all time points except 70 dpi, comparison to the results of Kneipp (Kneipp *et al.*, 2002) proved the successful reproduction of spectral alterations. Changes in the DMNV can be seen in the whole range between 1300 – 1000 cm^{-1} at the end of the disease: the width of the peak around 1240 cm^{-1} (asymmetric P=O stretching vibrations in PO_2 of nucleic acids and phospholipids) is slightly diminished in the DMNV of the infected animals. Changes can also be detected in the band shapes around 1170 cm^{-1} (asymmetric CO-O-C stretching vibrations of lipids). However, most

visible and earliest differences can be seen in the region of complex sugar vibrations of carbohydrates (~1060 - 1040 cm^{-1}).

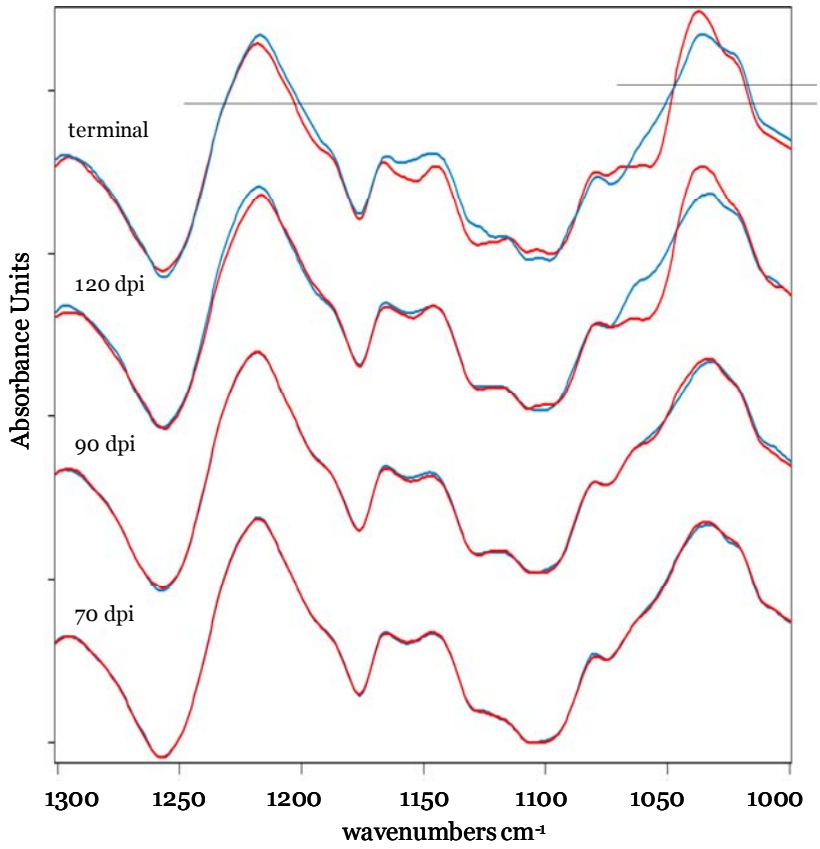

Figure 3.2.4: First derivative average spectra of scrapie-infected (red) and control animals (blue) at 70 dpi, 90 dpi, 120 dpi and at the terminal stage of disease (from bottom to top). Earliest and most prominent changes can be seen in the region 1100 – 1000 cm^{-1}.

Due to the dilution effect (see chapter 1.5.1) globular apertures of 50 µm covering large areas of the brain are probably too big to detect differences in protein composition induced by the presence of misfolded prion protein. Therefore, additional 5 scrapie infected and 3 control animals from the H100 hamster series (H100.01 H100.05 for infected and H100.21 – H100.23 for control) were studied at beamline U10B at the National Synchrotron Light Source (Upton, NY) using a synchrotron coupled spectrometer. In this way, higher spatial resolutions could be achieved with the aim to detect spectral differences in the protein and other molecular compositions of the samples. **Figure 3.2.5** shows the β-sheet distribution (middle row) and lipid composition (bottom row) of two 70 dpi control (left two columns, N100.21 and N100.22) and three 70 dpi infected animals (S100.02, S100.04 and S100.05). All animals derived from the H100 hamster series and were renamed into either S100 or N100 to show their infectious state (S=scrapie, N=normal). The corresponding

photomicrographs are plotted in the top row. For β-sheet distribution, red colored pixel correspond to areas with high β-sheet content, while blue correspond to those with low β-sheet. In all samples, areas near the cell's membrane exhibited highest amounts of β-sheet. In addition, the cytoplasm of infected cells, most prominent in animal S100.05 exhibited lower values of β-sheet compared to control. In the chemical images displaying the lipid composition (bottom row), red and yellow colored pixel correspond to areas with relatively high CH_3/CH_2 ratios, indicating longer fatty acid chains, while blue indicates areas with shorter fatty acids. In scrapie infected animals, spectral alterations indicating changes in the lipid composition towards shorter fatty acid chains can be seen in the animals S100.02 and S100.04 but not S100.05. This animal (S100.05), which exhibited the lowest amount of β-sheet but no spectral alterations that indicate changes in lipid composition, suggests that spectral changes in lipids and proteins might be time delayed events. Thus, the animals examined at 70 dpi could possibly be at individually different stages of this time dependent course of disease.

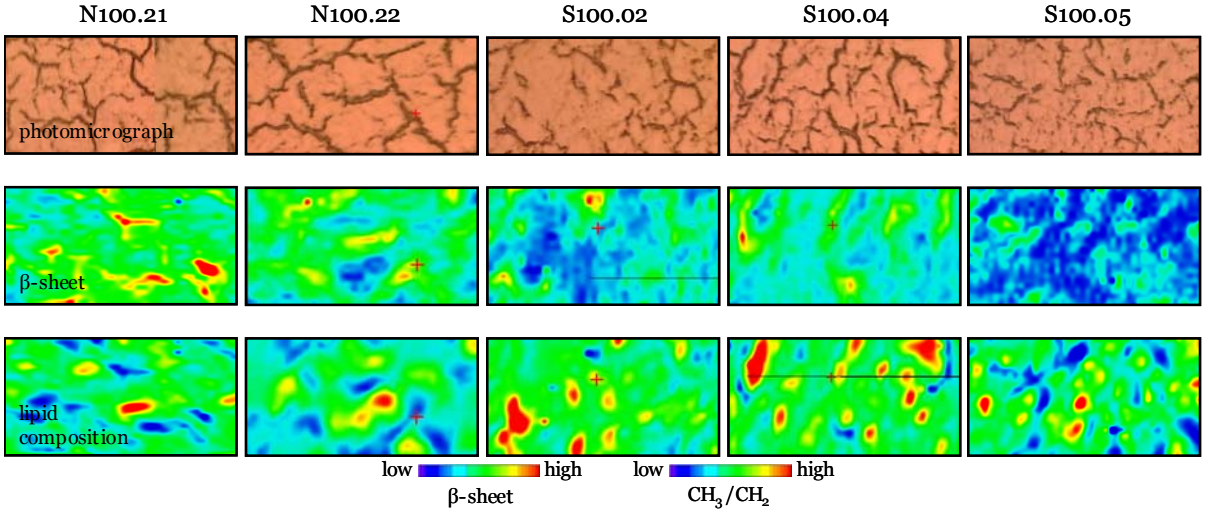

Figure 3.2.5: photomicrographs (top), β-sheet distribution (middle) and lipid composition (bottom row) of two control animals (H100.21 and H100.22, left) and three 70 dpi scrapie infected animals (H100.02, H100.04 and H100.05).Edge length red cross: 10 µm

Spectral indicators for changes in protein and lipid composition were subsequently analyzed quantitatively and are plotted in **Figure 3.2.6** (**C** and **D**, respectively), together with the total protein content (**A**) and the carbohydrate/phosphate analysis (**B**). While the β-sheet content slightly decreased, the amount of total protein slightly

increased, suggesting the up-regulation of proteins low in β-sheet. This was already detected in 100 dpi DRG (see **Figure 3.1.1 A** and **C**). Although differences in 70 dpi brains are smaller, these results suggest that early scrapie induced changes in the nervous system follow the same molecular events. The analysis of the fingerprint region revealed significant differences ($p = 0.0278$) between infected and control animals, arguing for changes in nucleic acids, carbohydrates and phospholipids to be the first disease related changes. In contrast, spectral indicators for changes in lipid composition does not show any differences when averaging over all animals.

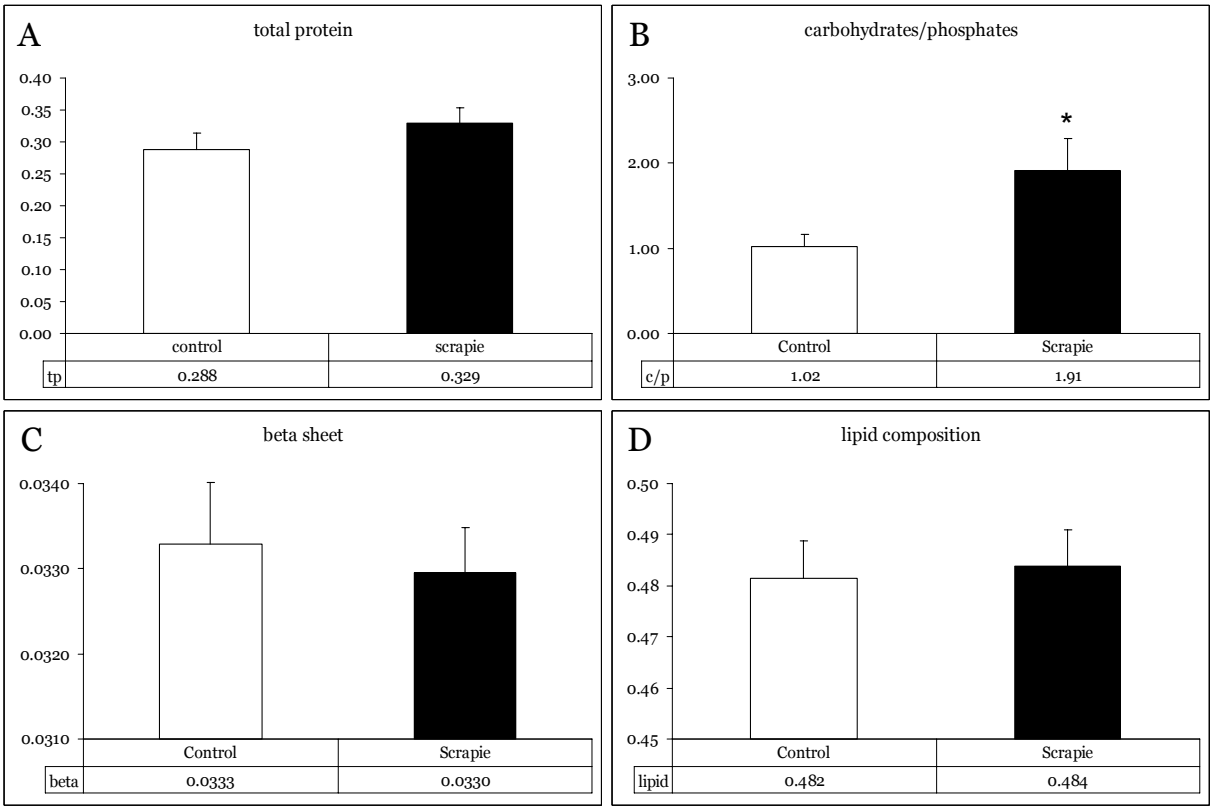

Figure 3.2.6: Results of the quantitative analysis of the total protein content (A), the carbohydrate/phosphate region (B), the β-sheet content (C) and the lipid composition (D) of five 70 dpi infected (black bars) and three control animals (white bars). *($p<0.05$)

3.3 DRG of terminally diseased 263K and ME7 infected hamsters

FTIR microspectroscopy has proven to be suitable to detect molecular alterations caused by prions in 263K scrapie challenged (orally) hamsters in multiple regions of the mid-infrared spectral range. To test the specificity of the induced changes, spectra of DRG of 263K infected animals have been compared to another strain, ME7, by using an FTIR spectrometer with a focal plane array as detector. Both strains are known to accumulate microdisperse aggregates of PrP^{Sc}. Since hamsters are not susceptible to oral inoculation with the ME7 strain, infection was carried out intracerebrally. In addition, the incubation time was about double from that of 273K (330 days compared to ~170 days). Finally it had previously not been known whether the ME7 agent enters the spinal cord and attached dorsal root ganglia and subsequently accumulates in those tissues. Therefore, Western Blot analysis of cervical and thoracic ganglia from terminally ill hamsters infected with 263K, ME7 or BSE-H (hamster adapted BSE strain) was carried out. As could been seen in **Figure 2.3.6** (see page 53), highest amounts for all three isolates were found in cervical ganglia compared to the thoracic, respectively. Furthermore, cervical ganglia of orally 263K infected hamsters seemed to have slightly higher amounts of PrP^{Sc} than cervical ganglia of ME7 infected, but less than those of BSE-H infected animals. Thoracic ganglia showed highest amounts of misfolded prion protein in 263K infected hamsters, higher than in ME7 and BSE-H. Based on the different infections, oral versus i.c., the spread of the agent in the nervous system is different. Nevertheless, spectra of the DMNV showed most β-sheet in the ME7 infected animals (see **Figure 3.3.1A**), highly significant compared to control ($p=0.0023$). The amount of β-sheet in 263K infected hamsters is lower than in ME7 but differences to control are still significant ($p=0.031$). In this calculation, 13.000 to 30.000 spectra each strain were investigated. Since the procedure of animal infection is different for the two strains, sites of first replication of the agent differ as well. While 263K enters the enteric system and from there, reaches the brain directly via the vagus nerve and indirectly over nerves originating in the thoracic area of the spinal cord, the ME7 agent starts to spread from the brain. It seems logical to find most β-sheet in areas where the agent appears first, and a comparison of β-sheet amount of different ganglia (thoracic 1,2,3,4 and 9) revealed that the closer the ganglion to the brain, the higher the amount of β-sheet in the tissue (see **Figure 3.3.1B**).

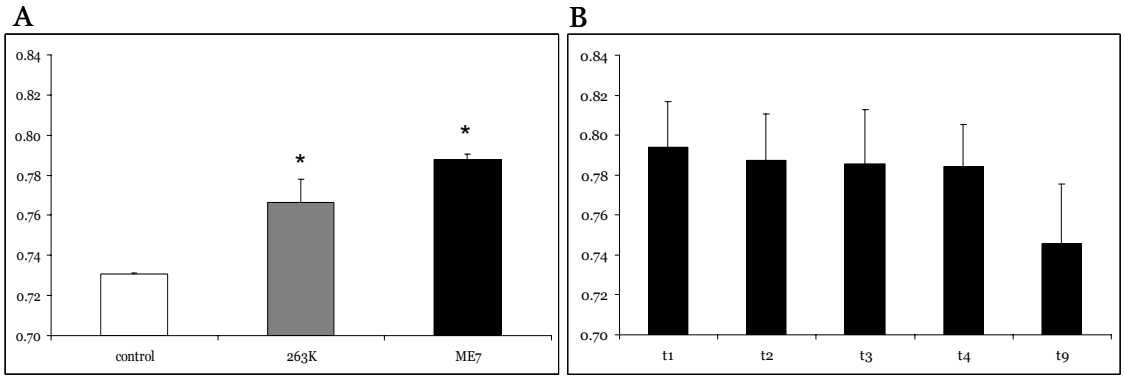

Figure 3.3.1: A. β-sheet to α-helix ratio of two control animals (19,949 spectra), four 263K (29,938 spectra) and two ME7 (12,956 spectra) infected animals. The 9th thoracic ganglion of one ME7 infected animal was excluded from the calculation. Asterisk indicates significant differences ($p<0.05$) between infected and control (263K: $p=0.0312$; ME7: $p=0.0023$) B. β-sheet to α-helix ratio of ME7 infected DRG in relation to the position of the ganglion (1st to 9th thoracic).

Although no quantitative analysis of the Western Blot analysis was performed, visible results suggested that ME7 does not exhibit higher amounts of PrP^{Sc} in the tissue, the detected changes in β-sheet amount might therefore be caused by other proteins high in β-sheet together with PrP^{Sc}. To identify the regions of elevated β-sheet in the tissue, chemical images of the β-sheet to α-helix ratio were generated and are shown exemplarily for one map each animal in **Figure 3.3.2**: The chemical image of one ME7 infected ganglion (left) shows mostly yellow coloring (ratio ~0.80) with some light green and red areas. Values below 0.7 were not observed. In comparison, the chemical image of the 263K infected animals (right) shows mostly appears green and shows less areas with elevated ratios. The control measurement (not shown) is dominated by blue-greenish colored pixels, indicating large areas with low sheet to helix ratios. In order to obtain higher spatial resolution than with the Perkin Elmer Spotlight instrument, measurements were also carried out on a Bruker Hyperion spectrometer (for details about determining the spatial resolution see the review by Lasch and Naumann (Lasch & Naumann, 2006)).

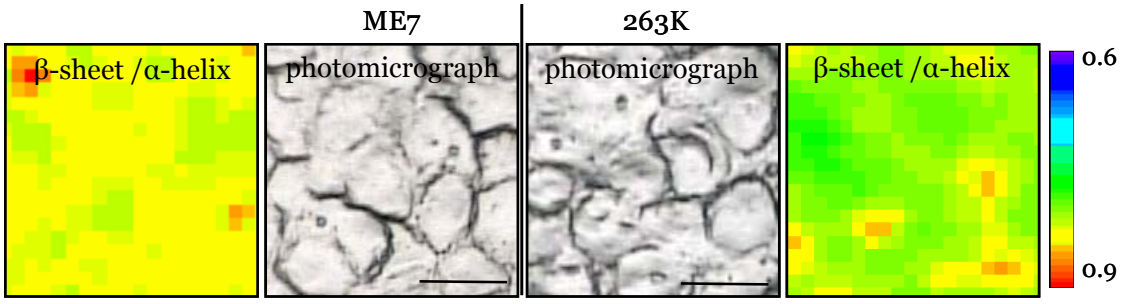

Figure 3.3.2: β-sheet to α-helix ratio of one ME7 (top), one 263K infected animal (middle) and one control (bottom) animal. Areas outside the ganglion (as seen in control) where excluded from the calculation. Scale bar: 50 µm

Chemical images of thoracic neurons of an ME7 infected animal (top), a 263K infected animal (middle) and a control animal (bottom) are shown in **Figure 3.3.3**. The chemical images are superimposed to the photomicrographs of the same area. Red and yellow pixels correspond to higher amounts of β-sheet and/or lower amounts of α-helix than green and blue. Original and 2nd derivative sample spectra representing high and low β-sheet to α-helix ratios are shown on the right. These spectra are averages as a result of a cluster analysis in the region 1800 – 1400 cm^{-1}. As can be seen in the control image, nervous tissue in healthy animals varies naturally in the amount of β-sheet. This variation, however, is lower than for the infected animals who show areas of high β-sheet rich proteins (or low α-helix) in neuronal cells, as can be seen by the red pixel. In addition, the cytoplasm of the cell shown in the control animal exhibit low ratios, while altered amide I band spectra seem to be more present at the cell's membrane. Neurons shown for the infected animals exhibit spectra with a downshifted peak maximum from about 1657 and 1656 cm^{-1} to ~1655 cm^{-1} (shown in red on the right), respectively, together with the appearance of a shoulder at around 1637 cm^{-1}. This has not been observed in any of the spectra from control animals. Furthermore, 2nd derivative spectra of ME7 and 263K derived neuronal tissue were compared with those from dried samples of purified proteins from the same strains (see **Figure 1.3** (Thomzig *et al.*, 2004)). For 263K, six peaks were apparent in the amide I band, which originates mainly from the >C=O stretching vibration of the polypeptide backbone (Krimm & Bandekar, 1986). These peaks were present at 1627, 1634, 1660, 1694 together with shoulders at 1669 and 1679 cm^{-1}. In contrast, 2nd derivative spectra of prion protein purified from brains of ME7 infected animals only revealed four peaks in the amide I region: at 1632, 1660-59, 1681 and 1694 cm^{-1}. Molecular vibrations absorbing in the region 1625 – 1620 cm^{-1} can be assigned to intermolecular hydrogen bond (>C=O) groups in β-sheets (Caughey & Raymond, 1991; Thomzig *et al.*, 2004), while the region between 1637 – 1630 cm^{-1} most likely indicates peptide >C=O groups rather involved in intramolecular β-pleated sheet structures (Krimm & Bandekar, 1986; Barth & Zscherp, 2002). α-helical structures are represented in the region between 1661 and 1656 cm^{-1} (Goormaghtigh *et al.*, 1990; Tamm & Tatulian, 1997) while a peak around 1694 cm^{-1} is assigned to the high frequency component of antiparallel β-sheet pleated structures (Krimm & Bandekar, 1986; Barth & Zscherp, 2002; Fabian & Mäntele, 2002). Finally, the region between 1681 – 1669 cm^{-1}, exhibiting a varying number of weak band components, is assigned to different types of turns or loop structures (Krimm & Bandekar, 1986; Barth &

Zscherp, 2002; Fabian & Mäntele, 2002). Comparing the spectra of dried purified prion protein with those derived from the nervous tissue reveals that peaks do not appear at the exact same locations. For example, a slight shoulder at 1628 cm^{-1} was observed in the tissue spectra of the ME7 cell but presented at 1632 cm^{-1} in the purified protein. The high frequency component at 1694 cm^{-1} and the shoulder at 1679 cm^{-1} in purified 263K prion protein are also shown in the spectra of the tissue, with minimal shift from 1694 to 1691 cm^{-1}. On the other hand, turns and loops presenting at 1681 cm^{-1} and high frequency β-sheet at 1690/91 cm^{-1} in ME7 infected tissue, have peak positions at 1681 cm^{-1} and 1694 cm^{-1}, respectively, in the purified proteins. At lower wavenumbers, the intra- and intermolecular β-pleated sheet structures are represented by peaks at 1639 cm^{-1} and 1630 cm^{-1} in 263K infected nervous tissue but were present at different wavenumbers in the spectra of purified protein (1634 and 1627 cm^{-1}).

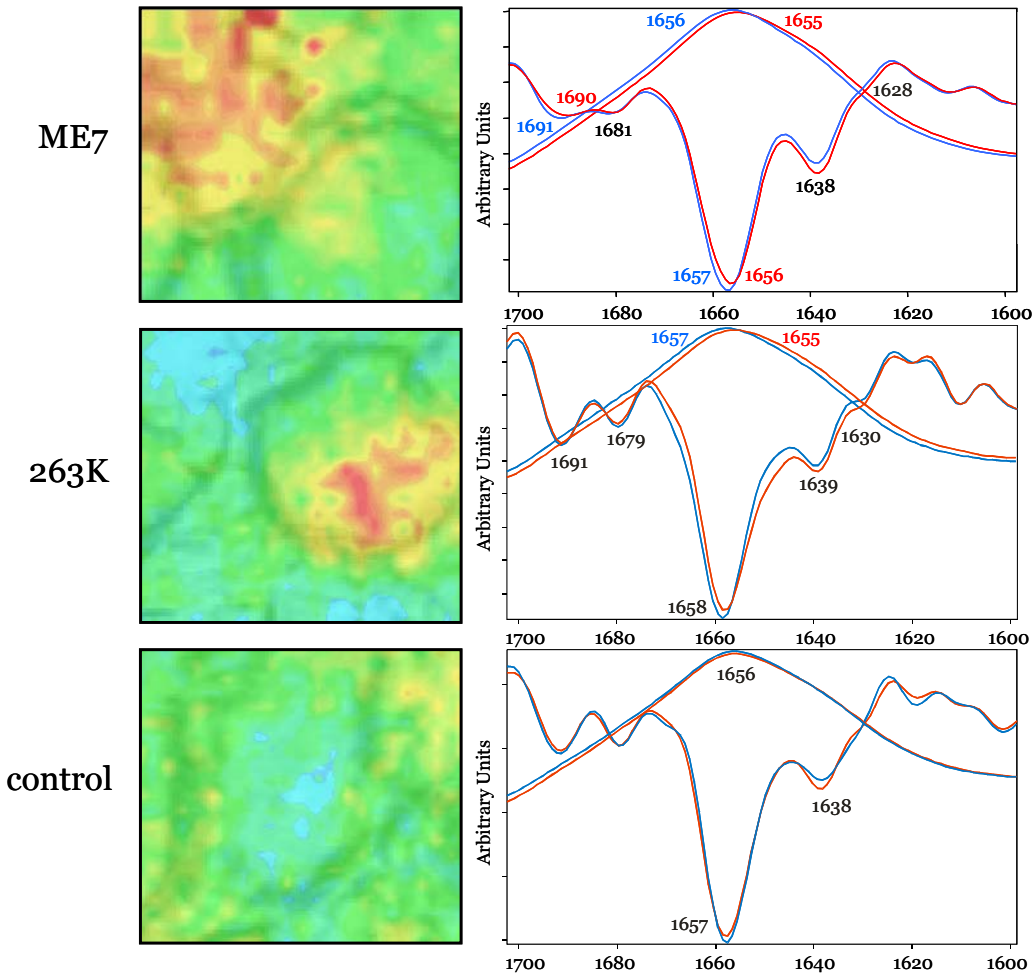

Figure 3.3.3: β-sheet to α-helix ratio of one ME7 (top), one 263K infected animal (middle) and one control (bottom) animal. The images are superimposed to the corresponding photomicrograph. Spectra of areas exhibiting high beta-sheet to alpha-helix ratios are shown in the corresponding right image (red spectrum) in original and 2nd derivative in the amide I band. Spectra of areas with low ratios are shown in blue. These spectra were generated based on a cluster analysis from 1400 -1800 cm^{-1} on vector-normalized original spectra.

All average spectra derived from cluster analysis in the region 1800 – 1400 cm^{-1} of vector-normalized original spectra showing altered amide I bands were in turn averaged. In this way, two spectra based on 6 maps of two 263K infected animals (H30.10 and H31.11) and 7 maps of two ME7 infected animals (H585.26 and H585.58) were generated and are shown in **Figure 3.3.4**. Spectra from ME7 infected and 263K infected animals are very similar. However, slight differences can be seen in the 2nd derivative spectra: ME7 shows increased peak intensities at 1691 cm^{-1}, associated with high frequency β-pleated sheet and 1639 cm^{-1} (intramolecular β-sheet) but decreased intensities at 1680 cm^{-1} (turns and loops), 1657 cm^{-1} (α-helix), 1630 cm^{-1} (intramolecular β-sheet) and 1610 cm^{-1} (possibly due to C=O and C=C stretching vibrations (M. M. Coleman, 1978)) in respect to 263K. However, these differences are very small probably due to the integrative nature of information provided by FTIRM.

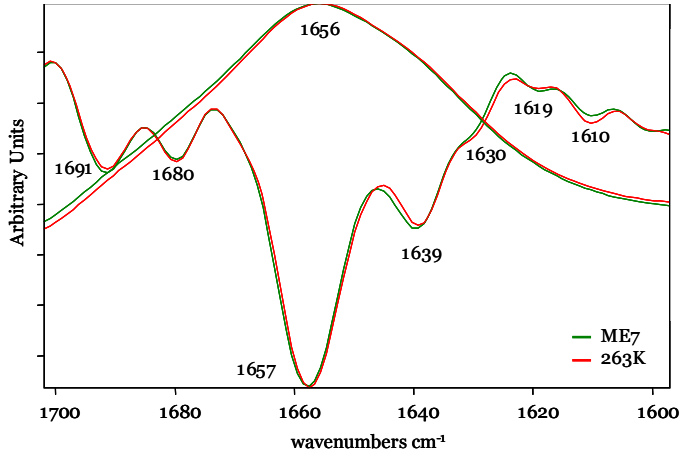

Figure 3.3.4: Original and 2nd derivative average spectra of two 263K infected (red) and two ME7 infected (green) animals.

First derivative spectra of averages calculated from two vector-normalized control animals (blue, thoracic ganglia 2-3), one 263K infected animal (red, cervical ganglion 2), three 263K infected animals (pink, thoracic ganglia 1, 5 and 6), two ME7 infected animals (green, thoracic ganglia 1-4) and one ME7 infected animal (light green, thoracic ganglion 9) are shown in the region 1300 – 1000 cm^{-1} plotted in **Figure 3.3.5A**. The thoracic 263K infected (pink) and the 9th thoracic ME7 infected ganglion (light green) only show small differences compared to the control ganglia and are very similar compared to each other. Differences can only be seen at 1216 cm^{-1}, where the spectrum of the 263K infected ganglion is slightly diminished compared to ME7 and a slightly shifted to lower wavenumbers from about 1040 cm^{-1} to 1039 cm^{-1}. Both peaks are slightly lower in the infected animals compared to control. More interestingly, the

ganglia closer to the brain, i.e. in 263K the cervical ganglia and in ME7 the 1st to 4th thoracic ganglia show remarkable differences compared to control. Here, differences in the slope of the spectra can be seen at the entire range between 1300 – 1000 cm^{-1} together with an additional peak at 1076 cm^{-1}. For better comparison, these spectra were shown separately as original vector-normalized spectra in **Figure 3.3.5B**. In 263K infected animals the peaks at 1238 cm^{-1} (originating primarily from nucleic acid phosphodiester groups) and 1171 cm^{-1} (CO-O-C asymmetric stretching arising from ester bonds in cholesterylesters and phospholipids) are decreased but increased at 1084 cm^{-1} (a multicomponent band including the symmetric phosphate stretching mode of nucleic acid phosphodiester groups; the C-O stretching mode of sugars and the C-O-P stretching modes of phosphorylated lipids, proteins and other molecules). The shoulder at 1062 cm^{-1} seems to be more prominent in ME7 infected animals. Changes in all of these peak intensities have been reported in early and late apoptotic cells (Jamin *et al.*, 2003).

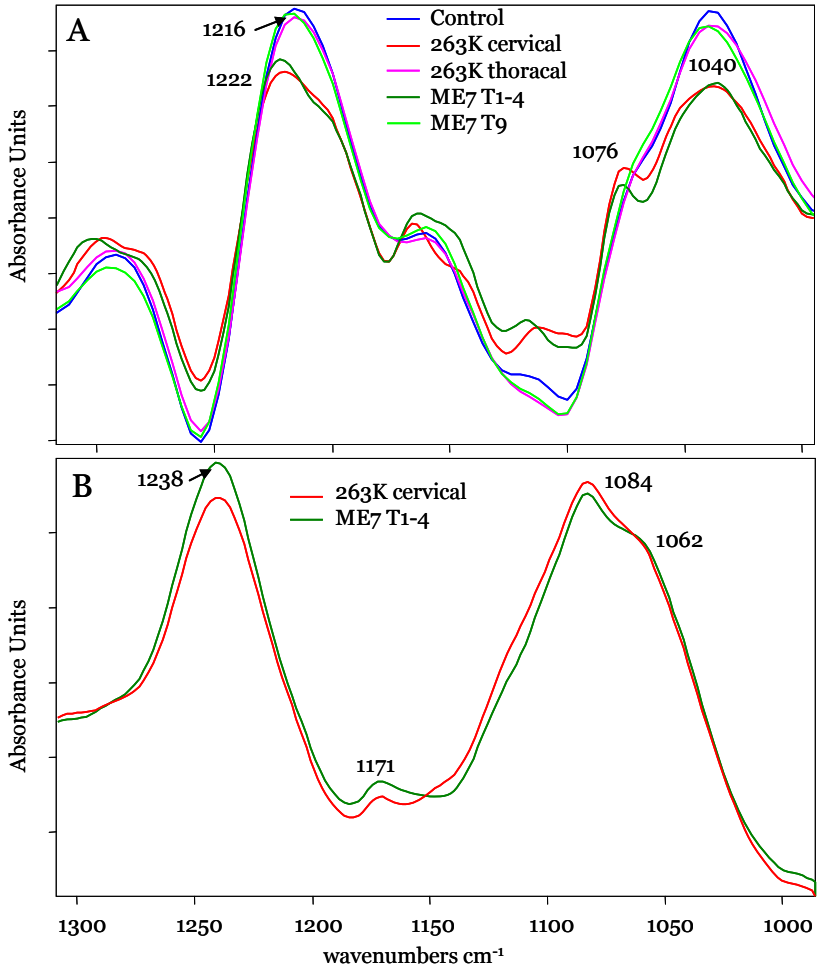

Figure 3.3.5: A. 1st derivative spectra of averages calculated from two control animals (blue, thoracic ganglia 2-3), one 263K infected animal (red, cervical ganglion 2), three 263K infected animals (pink, thoracic ganglia 1, 5 and 6), two ME7 infected animals (green, thoracic ganglia 1-4) and one ME7 infected animal (light green, thoracic ganglion 9) are shown in the region 1300 – 1000 cm^{-1}. B. Original average spectra of the cervical ganglion of one 263K infected animal (red) and the thoracic ganglion of one ME7 infected animal (green) shown in A.

To quantify spectral differences, the phoshpate/carbohydrate and the lipid region were analyzed for two control animals, four 263K infected and two ME7 infected animals as described in 2.6.6 and 2.6.7 (see page . In the fingerprint region (**Figure 3.3.6A**), scrapie 263K infected animals exhibited slightly higher ratios (1.54 in control to 1.62 in 263K) as was also detected by synchrotron FTIRM of DRG (1.34 to 1.44) and 70 dpi brain (1.02 to 1.91) in 263K scrapie and in reovirus infected animals (1.48 to 1.60). In contrast, terminally diseased ME7 infected animals exhibited significantly ($p=0.0265$) lower values compared to control animals. Additionally, the CH_3/CH_2 ratio was significantly increased in both 263K ($p = 0.0409$) and ME7 ($p = 0.0245$) (**Figure 3.3.6B**). The finding of an increased ratio in 263K infected animals is in conflict with the result of the synchrotron study, where the ratio was found to be slightly decreased (see **Figure 3.1.6A**). However, comparing the values revealed differences in the investigated controls to be bigger (0.485 with the FPA to 0.574 with the synchrotron) than those of the infected animals (0.0522 with the FPA to 0.567 with the synchrotron).

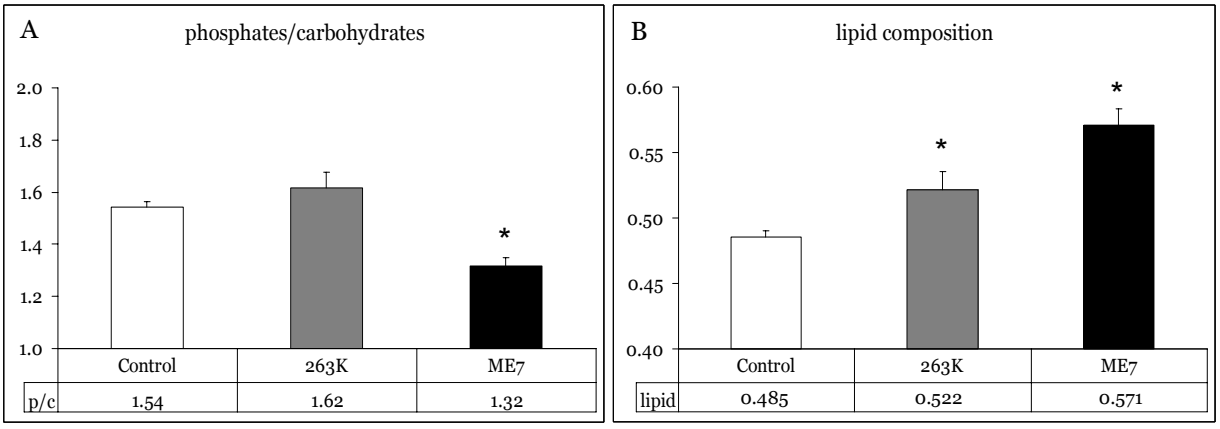

Figure 3.3.6: Quantitative Analysis of the phosphate/carbohydrate (A) and the lipid region (B) of two control animals (white bars), four 263K infected (gray bars) and two ME7 infected animals (black bars). *p<0.05

3.4 DMNV of Reovirus T3C9 infected hamsters

As mentioned, scrapie infection leads to spectral changes in the DMNV of infected animals not only at the terminal stage of the disease but already 90 (or even 70) days post infection. This fact leads to the inevitable question, whether the observed changes are specific for scrapie or whether another disease could cause the same spectral differences, i.e. molecular changes. A second approach to determine the specificity of the changes induced by 263K scrapie was the comparison of spectra of the DMNV to those derived from animals challenged with another neurodegenerative disease traveling the same pathway after oral inoculation. Therefore, hamsters were infected with Reovirus type 3 clone 9 (T3C9), causing a neurodegenerative disease that leads to fatal meningoencephalities in the challenged animal. Previous studies in mice have shown that infectivity is exclusively limited to newborn animals and that mice older than 2 days do not develop the disease (Derrien & Fields, 1999). This is the first time that newborn hamsters are shown to be susceptible for Reovirus T3C9 infection. Here, one day old Syrian hamsters, orally infected with 30 µl of virus suspension or medium only, respectively, developed a lethal encephalitis 9 days post infection. After sacrificing the hamster pups with Isofluran, FTIR measurements were carried out using a Bruker IFS28B spectrometer as described in 2.4.4. Coarse scans covering big areas of the Medulla oblongata ("Overview maps") were performed to identify the different structures in the tissue based on the protein/lipid-ratio. **Figure 3.4.1** shows an example of a cresyl violet stained section of the Medulla oblongata (**A**) and the corresponding chemical image based on the protein/lipid-ratio (**B**). Histological structures relatively high in protein content like the DMNV, the HypN and the area postrema distinguish from the lipid rich surrounding tissue by their green/yellow and red colored pixels. A detailed map was performed in the region shown in the black frame in the right image. The DMNV and the HypN can visually be identified in the stained picture, since the corresponding cell bodies are larger and less densely packed than those in the neighboring tissue structures. Higher detailed maps were conducted using a 50 µm circular aperture, 40 µm steps and 128 coadded scans per pixel spectrum.

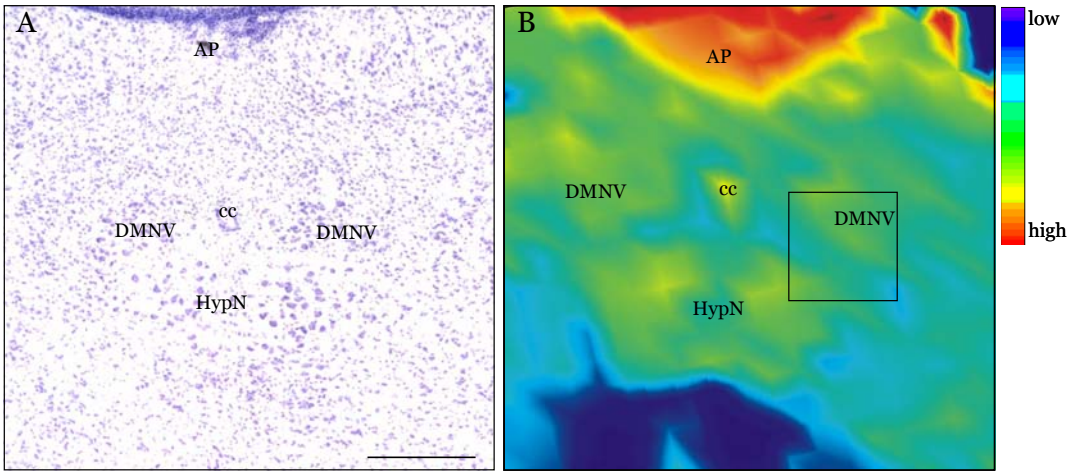

Figure 3.4.1: Cresyl violet stained photomicrograph of the Medulla oblongata of a 10 day old control hamster (A) showing the central canal (cc), the dorsal motor nucleus of the vagus (DMNV), the nucleus of the nervus hypoglossus (HypN) and the area postrema (AP). Scale bar: 500 um. The right side shows the protein/lipid ratio of the adjacent slide. Nuclei can be identified by the higher amount of protein from the surrounding tissue. The frame indicates the area that has been investigated in the detail measurement.

In Opus 5, Cluster Analysis on first derivatives in the spectral region 1300 – 1000 cm^{-1} were performed to separate the spectra of the DMNV from those of the HypN. Based on the original spectra, first derivatives were calculated using the Savitzky-Golay algorithm with 9 smoothing points and subsequently vector normalized in the region 1300 – 1000 cm^{-1} before clustering. **Figure 3.4.2A** shows the dendrogram of a control animal. It can be seen that the spectra within the subclusters, DMNV and HypN, are very similar but large differences exist between the two subclusters. First derivative average spectra of both clusters are shown in **Figure 3.4.2B**. Differences can be seen at ~1140 cm^{-1}, 1080 cm^{-1}, 1060 cm^{-1} and 1040 cm^{-1}.

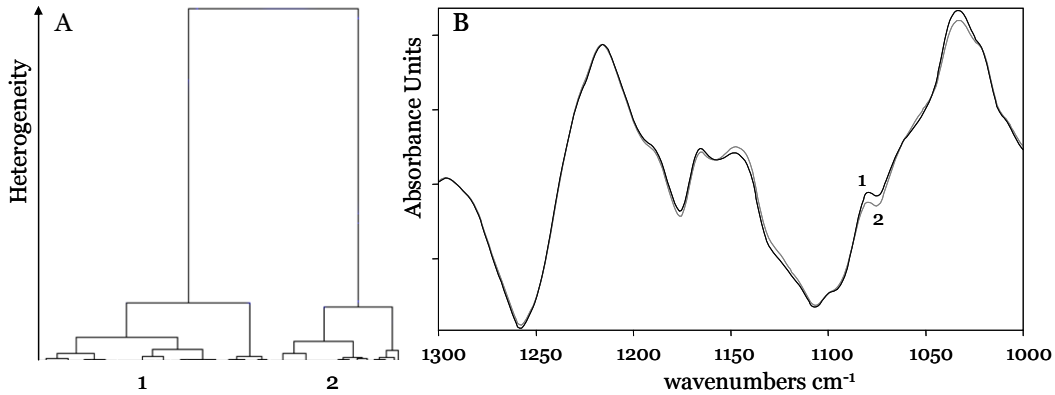

Figure 3.4.2: A. Dendrogram as a result of a Cluster Analysis of vector normalized first derivatives in the region 1300-1000 cm^{-1} of a detail map shown in Fig 3.5.1 B. B. Vector normalized first derivatives in the region 1300-1000 cm^{-1} showing the averages of the two main clusters displayed in A (DMNV = cluster 1; HypN = cluster 2).

The so separated average spectra of the DMNV of each animal, (seven infected and six controls), were in turn analyzed by cluster analysis. Here, the region between 1100 – 1000 cm^{-1} showed best clustering as can be seen in **Figure 3.4.3A**. Furthermore, 2 of the 6 control animals (N3 and N5) cluster together with infected animals, while the second cluster is composed of the remaining 4 controls. In order to analyze the molecular alterations occurring in reovirus infected animals, average spectra were created and are shown in **Figure 3.4.3B**. Interestingly, spectral differences are seen in the same region as for the scrapie infected animals, most prominently between 1100 – 1000 cm^{-1}, the region of complex sugar vibrations of carbohydrates. These alterations will be discussed in detail later.

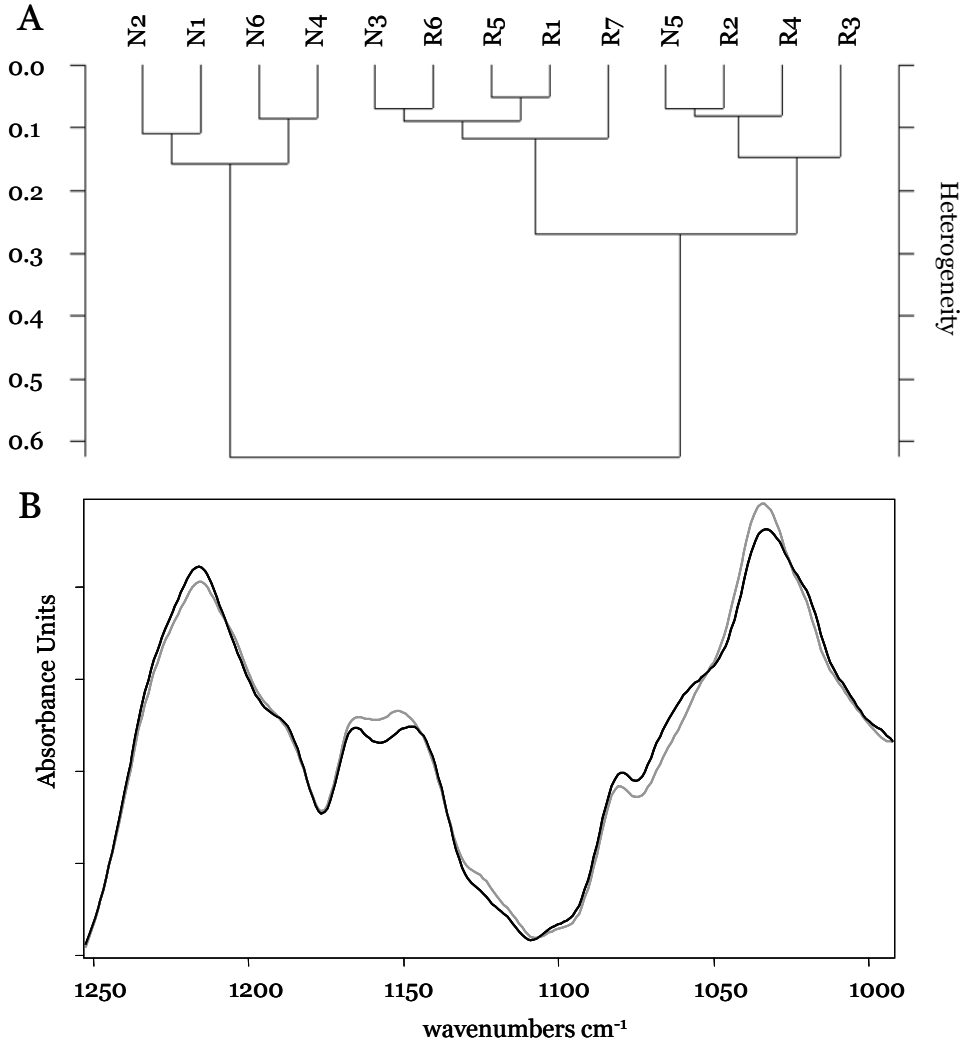

Figure 3.4.3: A. Dendrogram as a result of a cluster analysis on 1st derivative average spectra in the range 1100-1000 cm^{-1} of the DMNV from seven reovirus infected and six age matched control animals. B. 1st derivative average spectra of the seven reovirus infected (black) and six age matched control animals (gray) in the range 1300-1000 cm^{-1}

In addition, the amide I and amide II band of the average spectra were compared as well as the region between 3050 and 2800 cm^{-1}, where symmetric and asymmetric CH_2 and CH_3 stretching vibrations in lipids can be observed. No differences were observed in either the amide bands or the lipid region. However, virus infected animals show a prominent increase in peak intensity at 3013 cm^{-1}, which is associated with unsaturated fatty acids (**Figure 3.4.5**).

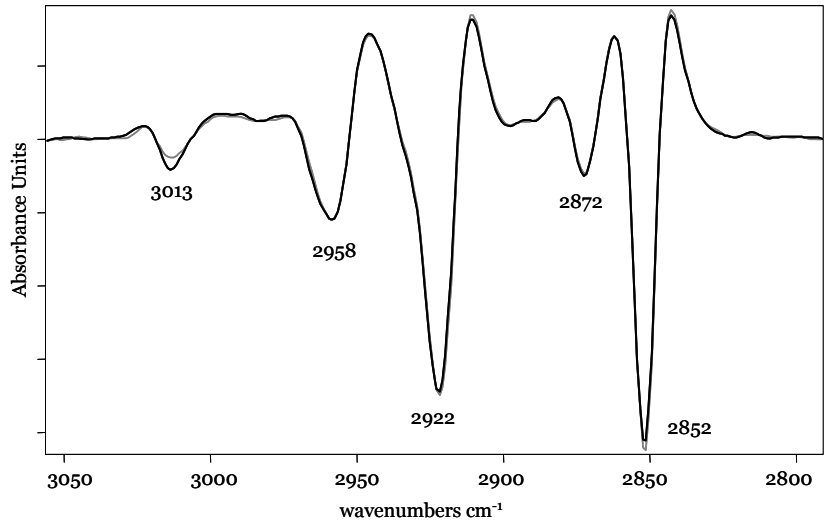

Figure 3.4.4: 2nd derivative spectra of the DMNV of reovirus infected (black) and control (gray) in the region 3050 – 2800 cm^{-1}. The spectra were vector normalized between 3050 – 2800 cm^{-1}. Differences can be seen at 3013 cm^{-1}.

To quantify spectral alterations, statistical analysis on all spectra was carried out in different regions of the original spectra: In the lipid region, analyzing the ratio of asymmetric CH_3 to CH_2 peak intensities (see **Figure 3.4.5A**), in the fingerprint region where mainly phosphates and carbohydrates absorb (the integrated area from 980 – 1149 cm^{-1} (baseline: 980 – 1149 cm^{-1}) divided by the integrated area from 1151 – 1350 cm^{-1} (baseline: 1151 – 1350 cm^{-1}), **Figure 3.4.5B**), and in the relative amount of proteins (protein content (integrated area: 1600 – 1700 cm^{-1}; baseline: 1480 – 1715 cm^{-1}) divided by the integrated area: 2700 – 3700 cm^{-1}; baseline: 2700 - 3700 cm^{-1}, figure **Figure 3.4.5C**). Assuming significant differences with $p<0.05$, the lipid composition ($p=0.0188$) and the phosphate/carbohydrate region ($p=0.0207$) are significantly altered in infected animals. Furthermore, reovirus infected animals showed slightly less total protein than controls.

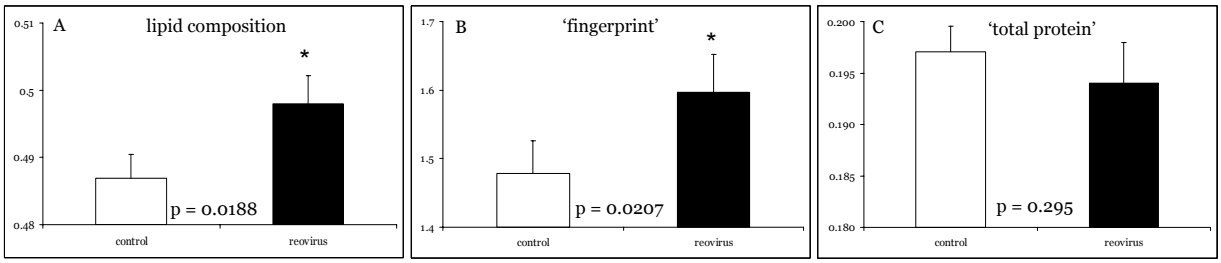

Figure 3.4.5: Statistical analysis of the lipid composition (A), fingerprint region (B) and total protein content (C) of six control (white bar) and seven infected hamsters (black bar). P-values calculated by a two sided unpaired t-test are shown in the graphs. *p<0.05.

3.5 Comparison of Reovirus to Scrapie induced spectral changes

Finally, the obtained average spectra were compared to average spectra of terminally scrapie infected and corresponding control animals (**Figure 3.5.1**). Changes occur in the same spectral regions in reovirus infected as in scrapie infected animals. However, between 1250 – 1200 cm^{-1} and 1100 – 1000 cm^{-1}, spectral changes are in the opposite direction. However, in the region around 1150 cm^{-1}, both diseases lead to similar changes in the corresponding average spectra. Higher "peak" intensities in first derivative spectra are partly due to sharper bands, i.e. smaller FWHH and partly due to different peak absorbance heights in the original spectra. Therefore, scrapie infection led to broader band shapes / lower peak absorbance height around 1240 cm^{-1} while reovirus infection sharpened the band / increased peak absorbance height of asymmetric P=O stretching vibrations in PO_2 of nucleic acids and phospholipids. Alterations in lipids, as seen around 1170 cm^{-1} (asymmetric CO-O-C stretching vibrations of lipids) may be independent of the type of infectious agent due to the same direction of spectral changes and just reflect general reactions of the body due to infection. One feature only detectable in scrapie infected animals can be seen at 1060 cm^{-1}, where complex sugar ring vibrations of carbohydrates absorb and might therefore reflect a scrapie specific molecular alteration. The nature of this potentially specific reaction in scrapie-infected animals, however, cannot be resolved by FTIRM. Furthermore it can be seen that in the region 1300 – 1100 cm^{-1} the scrapie infected animal and age-matched control on the one hand and the reovirus infected and age-matched control on the other hand are more similar to each other. This suggests that

disease related differences are smaller than age related differences and that it is not straightforward to compare diseased animals of different ages.

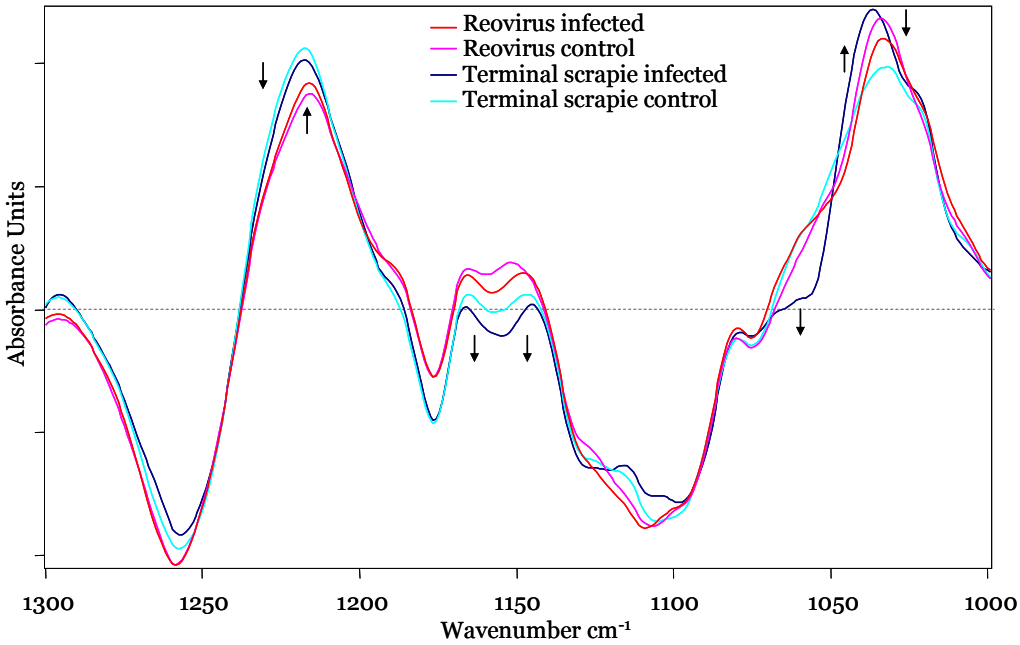

Figure 3.5.1: 1st derivative spectra of the DMNV of reovirus infected (red), age-matched control (pink), terminal scrapie infected (blue) and age-matched control (light blue) in the region 1300 – 1000 cm^{-1}. Arrows indicate direction of spectral changes from control to reovirus and from control to scrapie, respectively.

Analysis of control animals at three different ages revealed that spectra of those older than reovirus control and younger than terminal scrapie control are in the middle of both. Since scrapie is a neurodegenerative disease, spectral changes at ~1240 cm^{-1} might be due to neurodegeneration while the opposite changes occurring in reovirus infected animals are possibly due to "development", making those spectra more similar to those of older animals. At ~1150 cm^{-1}, both infections compared to control lead to the same direction of spectral changes. Here it is possible that the induced changes are caused by general immune responses of the challenged animal to the infectious agent. Finally, in the region 1050 – 1000 cm^{-1} of 1st derivative spectra, scrapie infected animals are more similar to young controls, suggesting that, like already mentioned for the peak at ~1240 cm^{-1}, infection with scrapie leads to neurodegeneration, making the spectra appear similar to those of young, undeveloped animals while infection with reovirus seems to cause a neuro"generation". It should be noted, too, that all reovirus infected and all age-matched control animals derived from the same dam. Naturally, pups are on different developmental stages when born and they are some more developed than others, especially the brain is not mature yet. It

needs to be noted that spectra were compared of animals at the same age but potentially different stages in their neurological development. Interestingly, control animals showed higher heterogeneity in the spectra of the DMNV than the reovirus infected animals who were more similar. This suggests that the infection with the virus causes molecular changes that "overlay" the spectrum and they would otherwise be more different to each other. The fact that two of the control animals cluster with the reovirus infected animals could be explained with the hypothesis that these animals were the most developed in the group of controls and that reovirus infection leads to spectral changes that are similar to those of developed, i.e. older, animals.

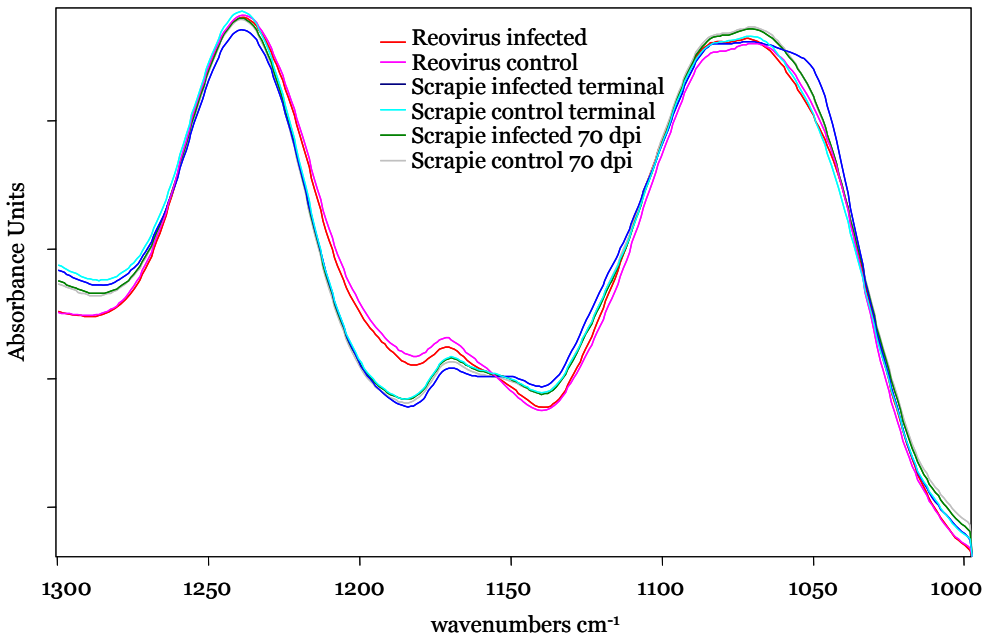

Figure 3.5.2: Original spectra of the DMNV of reovirus infected (red), age-matched control (pink), terminal scrapie infected (blue), age-matched control (light blue), 70 dpi scrapie infected (green) and age-matched control (gray) in the region 1300 – 1000 cm^{-1}.

To study possible age-related changes more detailed, original average spectra of two old animals (terminal scrapie infected and control, blue and light blue, ~200 days old), two middle aged animals (70 dpi scrapie infected and control, green and gray, ~100 days old) and two young animals (reovirus infected and control, red and pink, 10 days old) are shown in the region 1300 – 1000 cm^{-1} in **Figure 3.5.2**. At 1240 cm^{-1}, reovirus and 70 dpi infected animals are closer to their corresponding controls than controls to infected and are settled between terminal scrapie infected and age matched control. Only at the terminal stage, the peak at 1240 cm^{-1} in the terminal diseased animal is markedly decreased, probably due to the disease. Between 1170 – 1140 cm^{-1}, reovirus infected animals and their control are very different from the older animals.

Obviously, these differences are mainly due to the different ages of the hamster. In both cases infection leads to a decrease in the peak at ~1170 cm^{-1}. Reovirus infection leads to an increase at 1080 cm^{-1} and the disappearance of a shoulder around 1040 cm^{-1}. In contrast, scrapie infection does not cause changes at 1080 cm^{-1} but leads to a very prominent shoulder at 1040 cm^{-1}.

Cluster Analysis on vector-normalized 1st derivative spectra of infected and control animals of different ages and time points during the disease was performed in the region 1100 – 1000 cm^{-1}. The corresponding dendrogram is shown in **Figure 3.5.3**.

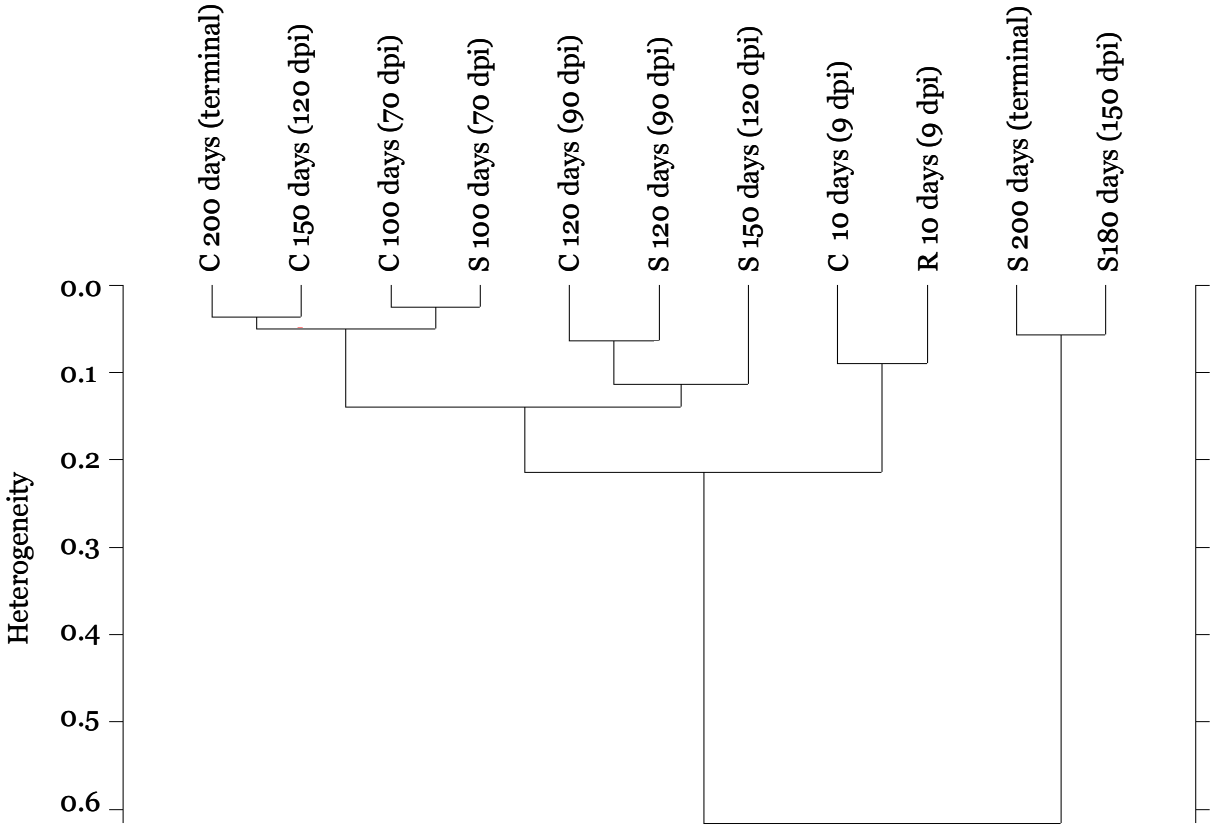

Figure 3.5.3: Dendrogram as a result of a cluster analysis on vector-normalized 1st derivative average spectra in the range 1100 - 1000 cm-1 of the DMNV from control animals of the ages 10, 100, 120, 150 and 200 days, scrapie infected animals at the ages 100, 120, 150, 180 and 200 days and 10 day old reovirus infected animals.

Control animals at the ages 10, 100, 120, 150 and 200 days, scrapie infected animals at the ages 100, 120, 150, 180 and 200 days and 10 day old reovirus infected animals were investigated. Although for control animals at the age of 200, 120 and 90 days and scrapie infected animals at the age of 200, 150, 120 and 90 days, only 1 animal each

was available, comparison of the spectra to those from an earlier study showed no differences (Kneipp, 2001). The result of the cluster analysis shows that terminal infected and 150 dpi scrapie infected animals form one cluster and all earlier time points in scrapie infected animals with their controls plus the reovirus infected animals and controls form the other cluster. This bigger group in turn clusters into very young animals, i.e. reovirus infected and control, and 100 – 150 days old scrapie infected plus 100 – 200 days old control animals. With the exception of late, i.e. 150 dpi and terminal scrapie infected animals, which cluster separately, the animals seem to group according to their age. Here, the very young animals, virus infected and control, separate from older animals, control and early, i.e. preclinical scrapie infection state. This indicates that scrapie induced changes at the beginning of the disease are smaller than age-related differences and only at late time points the induced changes are prominent enough to separate into distinct clusters.

3.6 XRF Microprobe pathogenesis study

To understand the possible correlation between trace metal distribution and prion protein misfolding, X-ray fluorescence (XRF) microprobe analysis was performed on the same ganglia that were studied with IR microspectroscopy. X-ray fluorescence involves excitation of the sample with an X-ray beam and measuring the fluorescence spectrum emitted. Different trace metals emit fluorescence at different energies, making the fluorescence intensity at a particular wavelength proportional to the concentration of the element that emits the fluorescent X-ray. One control ganglion and 2-3 infected ganglia at each time point (70, 100, 130, ~145 (fcs) and ~180 dpi (terminal)) were analyzed at beamline 2IDE at the Advanced Photon Source. Due to the low number of investigated animals, the obtained results can only serve as preliminary observations. Coarse scans covering areas of about 200 x 200 μm were recorded using a step size of 5 μm and a dwell time of 1 sec. Based on the corresponding photomicrograph as well as the iron and zinc distribution, orientation in the sample was possible and coordinates for subsequent fine scans were determined. Here, areas covering only about one to maximal four cells were recorded using a step size of 0.5 μm and a dwell time of 1 sec. Due to time constraints, coarse scans were analyzed for 70, 100, 145 and 180 dpi ganglia but fine scans only at the terminal stage. Here, the distribution of the elements copper, zinc, iron, calcium, manganese, and phosphorus were determined. The content of these elements over

time compared to age-matched controls are shown in **Figure 3.6.1**. Here it is shown that physiological concentrations of phosphorus are between 3-5 µg/cm², about a magnitude higher than that of calcium which in turn is about twice that of iron. Copper and zinc concentrations are about 2-3 times less than that of iron but about twice as much as manganese, the least abundant of the studied elements. Due to low animal numbers and normal individual variation, only severe differences were considered to be induced by the disease. Zinc (**Figure 3.6.1B**), iron (**3.6.1C**), manganese (**3.6.1E**) and phosphorus (**3.6.1F**) showed no differences from control at pre-clinical stages, while calcium (**3.6.1D**) and copper (**3.6.1A**) levels seemed to drop a little in scrapie infected animals before the terminal stage. **Figure 3.6.1A** suggests that copper levels decrease in control, i.e. healthy animals with age. Scrapie-infected hamster, however, followed this trend only until the animals reached the clinical phase. Then, infected animals did not decrease in copper content, leading to higher concentrations compared to age-matched controls. Zinc, similar to copper, showed decreased concentrations as the mock-infected animals aged. Again, only before the terminal stage, infected DRG exhibited similar zinc concentrations but did not decrease at the end of the time course, leading to higher concentrations of zinc in terminally infected animals (**3.6.1B**). Iron, both in infected and in control animals, did not seem to change over time, only at terminal stage, control animals exhibited slightly decreased levels while infected animals did not alter in their content (**3.6.1C**). In control animals, calcium levels, like copper and zinc, slightly decreased with age, while infected animals exhibited lower levels until and increased calcium levels at the terminal stage of the disease (**3.6.1D**). It should be noted that only one of the three investigated terminal scrapie infected animals contained much higher calcium levels than the control. Although the other two animals exhibited slightly lower calcium concentrations than the mock-infected hamster, the average value was still higher than in the examined control. Finally, manganese (**3.6.1E**) and phosphorus (**3.6.1F**) levels in healthy animals exhibited constant levels over time and only slightly de- and increased, respectively in older animals. In contrast, scrapie infected neurons remained constant levels over the whole investigated time, thus exhibiting higher levels of manganese and lower levels of phosphorus in terminal diseased animals.

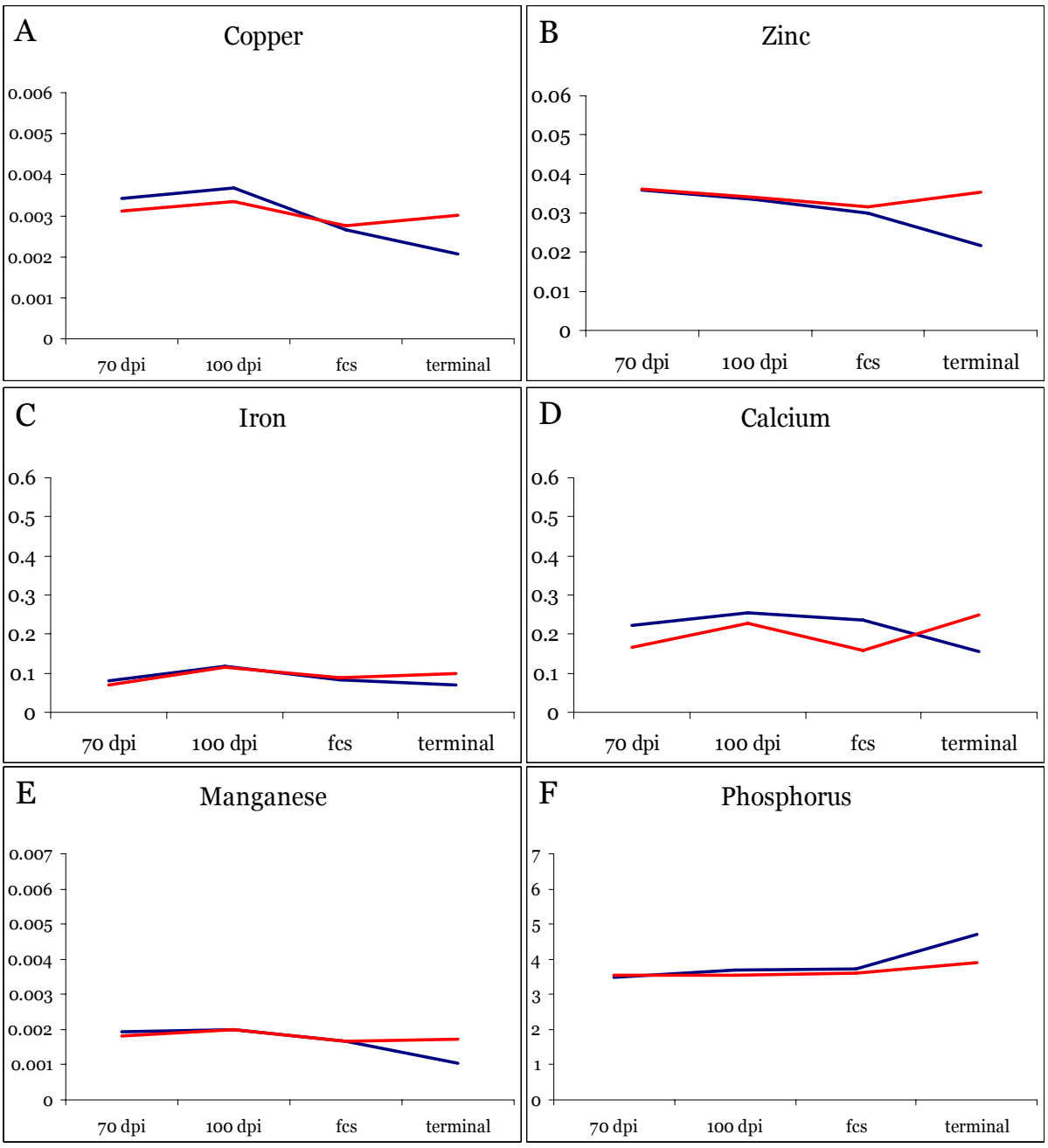

Figure 3.6.1: Cu (A), Zn (B), Fe (C), Ca (D), Mn (E), and P (F) content in µg/cm² in scrapie infected animals (red) compared to control (blue) over the course of the disease.

Figure 3.6.2 (bottom row) shows an example of a coarse scan of a control animal at terminal stage to demonstrate normal distribution of physiologically relevant elements. The upper four rows show (from top to bottom): one 70 dpi infected animal, one 100 dpi infected animal, one animal at fcs and one at the terminal stage. In general, copper and zinc concentrations are high intra- and lower extracellular, while iron and calcium are highest in the ECM. Manganese levels are generally low and due to undersampling of the sample in the coarse scans, i.e. bigger step size than beam size, conclusion about its cellular distribution was only possible from the fine scan (see

Figure 3.6.3). Here, manganese occurred highest in the cytoplasm and less in the nucleus and ECM. Quantification of elemental concentrations and image-processing was performed using MAPS software, and standardization to convert the fluorescence signal to a two-dimensional concentration in µg per cm² was achieved by fitting the spectra against the signal derived from thin-film standards NBS-1832 and NBS-1833 (National Bureau of Standards, Gaithersburg, MD). The columns display (from left to right) the photomicrograph of the measured area as well as the copper, zinc, iron, calcium and manganese distributions.

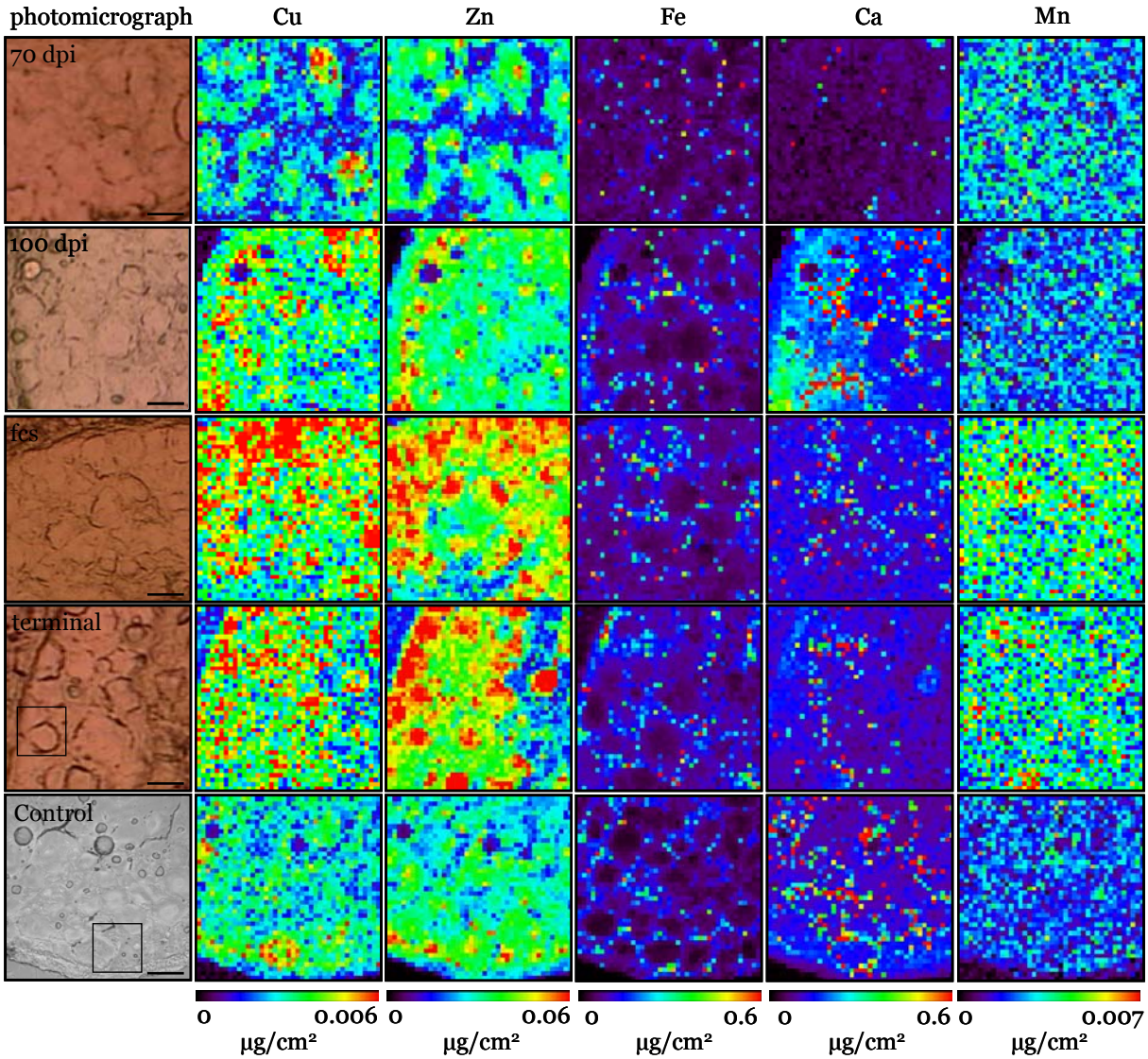

Figure 3.6.2: Cu, Zn, Fe, Ca and Mn content and distribution of a 70 dpi, a 100 dpi, a fcs, a terminal scrapie infected (from top) and one terminal control animal (bottom row) calculated from coarse scans. Squares in the control and terminal scrapie photomicrograph display the cell measured in the fine scan.

The rectangles shown in the photomicrographs represent the area of the fine scan which will be shown in the next figure. The distribution of the single elements are plotted in μg/cm², whereas red corresponds to areas with high concentrations and blue to those with low concentrations. Over the coarse of the disease, copper, zinc, iron and manganese increased in the shown scrapie infected animals. However, as seen in **Figure 3.6.1**, due to individual variations and low numbers of investigated animals, average values each time point and comparison to control slightly diminished that trend. Nevertheless, consistent with the previous figure, calcium levels in 100 dpi scrapie were increased compared to those at both 70 dpi and fcs, or, as **Figure 3.6.1** suggests, decreased in 70 dpi and fcs.

To investigate subcellular changes, fine scans with a beam size and step size of 0.5 μm were performed. For the fine scan maps, the analysis of elemental distribution was performed based on the subcellular structures nucleus, cytoplasm and extracellular matrix (ECM). The copper content for one map of the animals N32 (terminal control) and S14 (terminal scrapie) is presented in **Figure 3.6.3A**. In neuronal tissue, copper is present in highest amounts in the cytoplasm and slightly lower in the nucleus. Physiological variations of copper can be seen in the control image, where the cell shown in the left exhibits higher concentrations of copper in the cytoplasm than the cell shown to the right. In the scrapie infected cell, no changes in copper distribution can be seen but it appears that more cells show elevated content in the cytoplasm and/or nucleus. Zinc distribution was highest in the nucleus (**Figure 3.6.3B**) lower in the cytoplasm and lowest in the ECM. In scrapie infected cells, elevated zinc content was shown in the nucleus and/or cytoplasm. For iron, the distribution and average content is usually opposite to that of zinc, i.e. highest levels in the ECM (**Figure 3.6.3C**). Scrapie infected cells exhibited slightly higher intracellular concentrations of iron than the control. **Figure 3.6.3D** demonstrates the distribution of calcium which was shown to be similar to that of iron. Although **Figures 3.6.1D** suggest an increase in overall calcium content, no changes between scrapie and control could be seen in the map shown here. As already mentioned, the detected increase derived from one terminal infected animal (H100.11) that exhibited extremely high levels of calcium. The distribution of phosphorus is shown in **Figure 3.6.3E**, where control cells contained highest concentrations in the cytoplasm and lowest in the ECM. In scrapie infected cells, overall lower concentrations could been detected. Finally, the content and distribution of manganese is plotted in **Figure 3.6.3F**, showing overall very low

concentrations. In scrapie infected cells, however elevated manganese content was seen in the cytoplasm of some of the measured neurons.

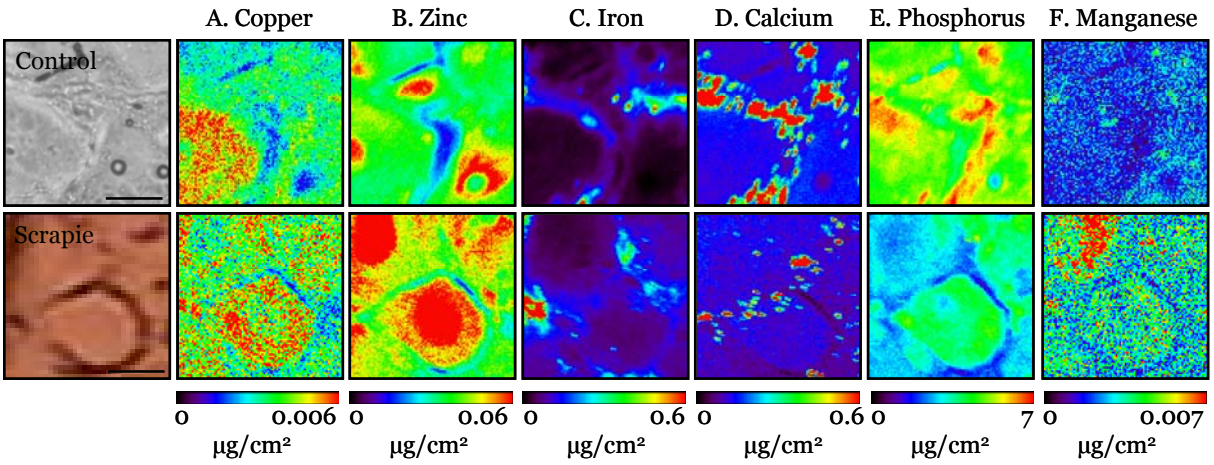

Figure 3.6.3: Cu (A), Zn (B), Fe (C), Ca (D), P (E) and Mn (F) distribution in neurons of one a control animal (top) and one terminally diseased animal (S14, bottom) derived from the fine scans. Red and yellow corresponds to high, green and blue to low concentrations.